

Saturation Physics of Threshold Heat-Flux Reduction

P.-Y. Li¹, P.W. Terry¹, G.G. Whelan¹, and M.J. Pueschel^{2,3}

¹*Department of Physics, University of Wisconsin-Madison, Madison, Wisconsin 53706*

²*Dutch Institute for Fundamental Energy Research, 5612 AJ Eindhoven, The Netherlands*

³*Eindhoven University of Technology, 5600 MB Eindhoven, The Netherlands*

Abstract

The saturation physics of ion-temperature-gradient-driven turbulence is examined in relation to the temperature-gradient variation of the heat flux, which can exhibit an upshift of the critical gradient for significant flux relative to the linear instability threshold. Gyrokinetic measurements of saturation properties and spectral energy transfer (which will be defined in Sec. II) are presented, indicating that the physics of saturation is fundamentally unchanged on either side of the upshifted gradient. To analyze heat transport below and above the upshifted critical gradient, a fluid model for toroidal ITG turbulence is modified to include the kinetic instability threshold. The model and the heat flux are rendered in the eigenmode decomposition to track the dominant mode-coupling channel of zonal-flow-catalyzed transfer to a conjugate stable mode. Given linear and nonlinear symmetries, the stable mode level and the cross correlation of the unstable and stable mode amplitudes are related to the unstable mode level via linear physics. The heat flux can then be written in terms of the unstable-mode level, which through a nonlinear balance depends on the eigenmode-dependent coupling coefficients and the triplet correlation time of the dominant coupled modes. Resonance in these quantities leads to suppressed heat flux above the linear threshold, with a nonlinear upshift of the critical gradient set by the resonance broadening of finite perpendicular wavenumber and collisionality.

1 Introduction

Improving plasma confinement has remained a critical goal for magnetically confined fusion plasmas for decades [1]. A chief concern has been confinement losses associated with microturbulence. Despite significant progress in identifying and utilizing strategies for reducing losses associated with turbulence [2, 3, 4], new devices such as ITER and SPARC [5] have stringent specifications for transport relative to empirical benchmarks, and their achievement will require effort and skill on the part of experimenters. Beyond reaching overall confinement milestones, there is considerable advantage in being able to achieve transport control with selectivity relating to both location and time [4]. To achieve such advances, it will be necessary to thoroughly understand the plasma turbulence associated with confinement losses. Such understanding will furthermore enable transport reduction strategies through the design of three-dimensional magnetic fields in stellarator configurations [6], including those that seek lower transport levels by improving the efficiency of nonlinear energy transfer [7].

There is a well-known but poorly understood transport-reduction phenomenon whose study represents an opportunity to better understand the saturation of important micro-instabilities and physics that lowers transport rates. We refer to the so-called Dimits shift, the onset of significant heat transport at the nonlinear critical gradient (NLCG), a higher gradient than the linear instability threshold [8]. In the region below the NLCG but above the linear threshold, the heat flux is low relative to expectations based on linear drive strength but not zero, representing a gradient range of strongly but not completely suppressed transport. This phenomenon is observed in nonlinear simulations of ion-temperature-gradient-driven (ITG) turbulence with both gyrokinetic [9] and fluid models [10]. It also occurs for density-gradient-driven trapped electron turbulence [11]. We argue that the upshift is an integral part of the mechanism for saturation of ITG turbulence that has already been studied above the NLCG [12]. This mechanism involves the transfer of energy to stable modes through the zonal flow. When included in a model with the physics of the linear instability threshold, this mechanism reproduces many features of the critical-gradient upshift [10]. It is also consistent with detailed analyses of gyrokinetic simulations described in Sec. 2, which

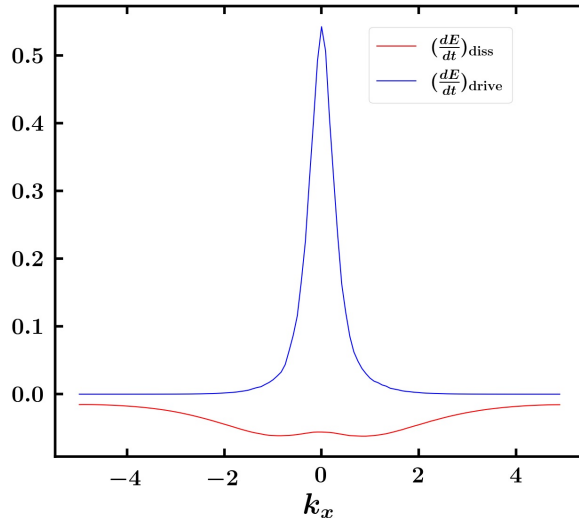


Figure 1: The energy drive and energy dissipation averaged over z and time, and summed over k_y as a function of k_x . Over the wavenumbers plotted, the energy dissipation rate is much larger within the unstable range than outside it. The absolute values of the total area under both curves are ≈ 4.78 .

suggest that salient aspects of the saturated state are qualitatively the same on either side of the NLCG.

Despite numerous attempts to understand the critical-gradient upshift, none is considered definitive [13, 14, 15, 16, 17, 18, 19]. Suppression of transport below the NLCG by zonal-flow shearing has been a recurring theme, a notion that requires zonal-flow shearing to lose effectiveness above the NLCG [13, 14, 15, 16]. While zonal flows are excited in ITG turbulence and are known to reduce turbulence levels [8], they do this primarily by enabling energy transfer to stable modes [20, 21]. As shown in Sec. 2, the zonal-flow shearing hypothesis is at odds with a number of observations of the nonlinear turbulent state in gyrokinetics. Other mechanisms for the critical-gradient upshift involve adjustments of spatial fluctuation structure to inhomogeneous zonal flows with non-uniform shear [19], or aspects of mode coupling [22]. Numerous results have shown that the large-scale stable modes are critical in the saturation of ITG turbulence [12, 23, 24], however, those are not taken into consideration in these mechanisms.

ITG turbulence has been well characterized by observations from gyrokinetic and fluid simu-

lations. While most observations are made above the NLCG, we will show in Sec. 2 that turbulence features remain similar below the NLCG. Key features include the following. 1) In the wavenumber range of instability there is a large removal rate of fluctuation energy by nonlinearly excited stable modes [25]), which can be seen in Fig. 1, where the result is derived from an adiabatic-electron Cyclone-Base-Case GENE simulation with $\omega_{T_i} = 7$ (in units of R_0/L_{T_i} , the ratio of major radius and temperature gradient scale length). 2) Due to the stable modes, energy transferred toward small scales is mostly removed from the spectrum before reaching the largest wavenumber of the unstable range. This is demonstrated in Fig. 1 of Ref. [26], where it should be noted that inertial transfer, i.e., no energy removal by the stable modes, would yield constant transfer rates. The energy transfer rate will be explicitly defined in Sec. 2. 3) Energy transfer to the stable modes goes through the zonal flow, and its rate matches the energy input rate from the instability (see Fig. 9 of Ref. [20]). Net energy uptake by the zonal flow is small ($< 10\%$) in relation with the energy transferred to the stable mode. 4) The triplet decorrelation rate of the interaction of unstable mode, stable mode, and zonal flow, which mediates saturation, is a minimum relative to that of other interactions (see Fig. 13 of Ref. [20]). These features need to be accounted for in theories of the critical-gradient upshift.

These observations contradict foundational tenets of the shearing paradigm for zonal-flow regulation. Consider, for example, the wave-action-invariance argument of zonal-flow regulation via shearing [27]: shearing enhances energy transfer to $k_x > 1$ (here and throughout this paper wavenumbers are all normalized with the ion sound gyroradius ρ_s); energy at these scales then lowers the wave frequency, which in turn lowers wave energy to maintain invariance of wave action; lower wave energy is then offset by an increase in zonal flow energy, which through its shearing perpetuates the process. The underlying premise of wave-action invariance is invalidated by the sizable large-scale dissipation seen in Fig. 1. The subsequent effects of the wave-action-invariance argument are contradicted by observation: most cascaded energy fails to reach even $k_x = 0.5$ before being removed from the system, the zonal flow only takes up a small fraction of transferred energy, and the nonlinear decorrelation rate is minimized, while in the shearing hypothesis it increases.

Our analysis of saturation below and above the NLCG starts with nonlinear simulations using the gyrokinetic code GENE [28]. We find that the heat flux below the NLCG increases slowly relative to the growth rate, then smoothly but rapidly increases its slope near the NLCG. The latter is not precisely defined or indicative of a bifurcation, as evident from continuously varying nonlinear energy transfer rates that set fluctuation levels. Both direct transfer in single sets of wavenumber triplets and cascading transfer through a series of triplets are qualitatively the same below and above the NLCG. Moreover, the character of this transfer will be shown in Sec. 2 to be consistent with saturation by stable modes accessed via zonal flows. Both the zonal-flow shearing rate and the ratio of shearing rate with linear growth rate are larger above the NLCG than below it.

Consistent with these results, we develop a theory for the heat flux that is valid below and above the NLCG [10]. Both regimes are nonlinear and will be called the low and high transport regimes, respectively. The theory is based on a tractable nonlinear fluid model [12] modified to recover the linear dispersion relation and instability threshold condition of a drift-kinetic calculation [29]. Low and high transport regimes naturally emerge from a single saturation mechanism — energy transfer through the zonal flow to stable modes. This interaction is nearly resonant, producing weak transport near threshold. Transport increases sharply at higher gradients due the gradient dependencies in resonance-broadening effects.

The heat flux depends on the fluctuation levels of unstable and stable modes, and the complex-valued cross-correlation of the two modes. We solve for these quantities using conjugate symmetry and nonlinear energy conservation. The relationship between levels of unstable and stable modes is consistent with dissipation-rate equipartition [24]. Because of nonlinear symmetry that leads to the cancellation of nonlinear terms affecting the eigenmode cross correlation, its phase depends mostly on linear physics. With these relationships, a single saturation balance suffices to determine the heat flux. This balance is solved accounting for all eigenmode levels and explicitly handling wavenumber variation using a Markovian procedure.

The near-resonant effects that suppress the flux just above the linear threshold include a

complex-wave-frequency resonance from the correlation time of the triplet interaction, a measure of the nonlinear interaction lifetime, of the unstable mode, zonal flow, and stable mode. In the limit that the collisionality and perpendicular wavenumber go to zero, the linear part of the correlation time goes to infinity, which allows a vanishingly small turbulence level to match the energy input of the instability, resulting in zero heat flux. The resonance is broadened by collisionality and the ion polarization drift, both of which give a small residual heat flux that increases with temperature gradient. The nonlinear coupling coefficient, which is a function of eigenmode frequency, also contributes to the small heat flux just above the linear critical gradient, and its eventual steep rise at larger gradient values.

This paper is organized as follows. Section 2 describes gyrokinetic observations of turbulence in the low and high transport regimes. In Sec. 3, a fluid model for toroidal ITG turbulence is introduced, modified to match a kinetic dispersion relation and its critical gradient for instability, and transformed to the eigenmode decomposition. In Sec. 4, the relationships between eigenmode amplitudes and the eigenmode cross correlation are derived and used to obtain a succinct expression for the heat flux in terms of the unstable mode level. Statistical closure theory is applied in Sec. 5, and an expression for the eddy damping rate associated with zonal-flow-catalyzed transfer is derived. The nonlinear balance for the overall turbulence level is solved in Sec. 6 and used to obtain a heat flux expression valid in low and high transport regimes. Section 7 provides concluding remarks.

2 Comparative Turbulence Analysis

While the heat flux and turbulence levels are small in the low-transport regime, they are not zero. This can be seen in Fig. 2, where the linear critical gradient is $\omega_{T_i} \approx 4.75$ and the NLCG is $\omega_{T_i} \approx 6.5$. Given these values, $\omega_{T_i} = 5.5$ is in the low-transport regime, $\omega_{T_i} = 6.5$ is around the NLCG, and $\omega_{T_i} = 7$ is above the NLCG. Gyrokinetic simulations show that in many respects, aside from overall levels, the turbulence in the low and high transport regimes is very similar. Figures 2–5 show results from analyses of gyrokinetic simulation data obtained with the turbulence code GENE [28] for the parameters of the collisionless adiabatic-electron Cyclone-Base-Case [8]. The

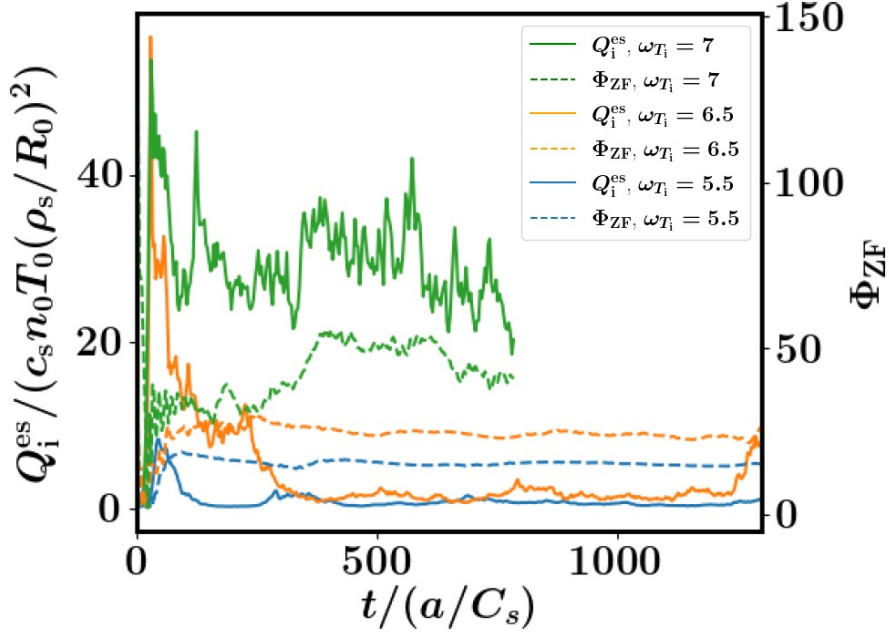


Figure 2: Time history of Q_i^{es} and Φ_{ZF} for saturated ITG turbulence from gyrokinetic simulations for $\omega_{T_i} = 5.5$, $\omega_{T_i} = 6.5$, and $\omega_{T_i} = 7$. The NLCG is at $\omega_{T_i} \approx 6.5$.

GENE simulation details can be found in the appendix of Ref. [30]. In Fig. 3, the energy spectrum

$$E_k = \text{Re} \left\{ \sum_j \int \frac{n_{j0} T_{j0}}{F_{j0}} \left[g_{j,k} + \frac{q_j F_{j0}}{T_{j0}} \chi_{j,k} \right]^* g_{j,K} dz dv \right\}, \quad (1)$$

is plotted as a function of k_x and k_y , the radial and poloidal wavenumbers, respectively, where $g_{j,k}$ is the nonadiabatic distribution function for species j with wavenumber k , $\chi_{j,k}$ is the modified potential (which, in general, is comprised of both electrostatic and electromagnetic component), n_{j0} is the background density, $T_{j,0}$ is the background temperature, q_j is the charge, F_{j0} is the background Maxwellian, z is the parallel coordinate, and v is the velocity. The plots represent two values of the temperature gradient ω_{T_i} , with $\omega_{T_i} = 5.5$ for a), while for b) $\omega_{T_i} = 7$. In a) the $k_y = 0$ energy is plotted at 0.01 of its actual value, while in b) the $k_y = 0$ energy is plotted at 0.1 of its actual value. The spectra are qualitatively similar. Below the NLCG the spectrum extent is somewhat more restricted in k_x and k_y , and the peak is shifted moderately to higher k_y . Both of these tendencies are well-matched to the growth rate spectra at the two values of ω_{T_i} , which show reductions of peak growth rate and unstable range by a factor of ~ 2 for $\omega_{T_i} = 5.5$ relative to $\omega_{T_i} = 7$ [30].

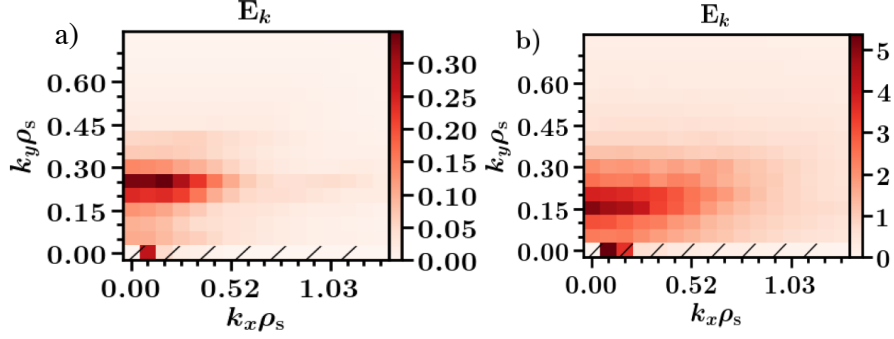


Figure 3: The time-averaged energy spectra of the ITG turbulence for saturated gyrokinetic simulations for a) $\omega_{Ti} = 5.5$ and b) $\omega_{Ti} = 7$. The NLCG is at $\omega_{Ti} \approx 6.5$. Both show strong band structure in the k_x direction, and modes are only strongly excited in the low- k regime. To better see how energy is distributed the $k_y = 0$ energy is plotted at 0.01 of its actual value in a), while the $k_y = 0$ energy is plotted at 0.1 of its actual value in b).

In Fig. 4, spectral energy transfer rates $\langle T_{k,k'} \rangle$ are plotted, again for $\omega_{Ti} = 5.5$ and 7, where

$$T_{k,k'} = 2\text{Re} \left\{ \sum_j \int \frac{n_{j0} T_{j0}}{F_{j0}} \left[g_{j,k} + \frac{q_j F_{j0}}{T_{j0}} \chi_{j,k} \right]^* (k'_x k_y - k_x k'_y) [\chi_{j,k'} g_{j,k''} dz dv] \right\}, \quad (2)$$

the angle brackets represent the time average, and $k'' = k - k'$. The energy transfer rate into each grid cell is registered by color. Energy is transferred directly from the mode $(k_x, k_y) = (0, 0.2)$. Thus in Fig. 4 a) energy is removed from $(k_x, k_y) = (0, 0.2)$ and deposited into $(k_x, k_y) = (0.086, 0.2)$. Energy transferred from $(k_x, k_y) = (0, 0.2)$ to the cells with $k_x > 0.086$ and $k_y = 0.2$ is very small. In Fig. 4 b) energy is removed from $(k_x, k_y) = (0, 0.2)$ and deposited into a number of cells to its right, with significant energy going into $(k_x, k_y) = (0.086, 0.2)$ and $(k_x, k_y) = (0.172, 0.2)$ and a much smaller quantity going to cells with $k_x > 0.172$ and $k_y = 0.2$. This prominent horizontal feature represents transfer to modes with $k_y = 0.2$ and various k_x , and requires coupling to the zonal modes $(k_x, 0)$. Its prominence reflects the fact that zonal-flow-catalyzed transfer is the dominant transfer channel. Transfer in the low and high transport regimes is similar; the greater extent of $\langle T_{k,k'} \rangle$ in k_y is consistent with a stronger and broader growth rate spectrum above the NLCG.

Fig. 5 shows the energy transferred from modes $(0, k_y)$ to wavenumbers on horizontal bands at different k_y through a sequence of interactions with the zonal flow $(0.086, 0)$. The sequence represents energy moving to higher k_x at a single $k_y = 0.2$ by increments of $\delta k_x = 0.086$, with color measuring the transfer in each step of the cascade, i.e., into a given cell from the cell immediately

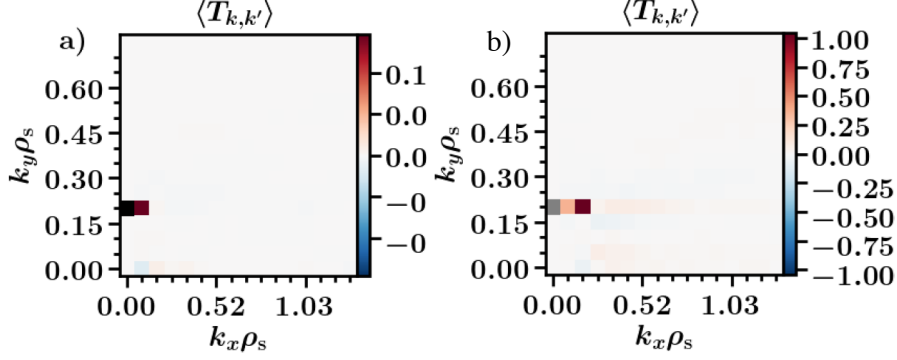


Figure 4: The time-averaged rate of direct energy transfer from $(k_x, k_y) = (0, 0.2)$ to grid cells for a) $\omega_{T_i} = 5.5$ and b) $\omega_{T_i} = 7$ at saturated state. The prominent horizontal bands for $k_y = 0.2$ represent the major energy transfer channel is the zonal-flow-catalyzed energy transfer.

to its left. A tabular representation of the data involved in making a figure like Fig. 5 is given in Ref. [21] (Fig. 2). The energy measured is associated with the squared fluctuating distribution function $g_{j,k}$, a quantity that is sometimes called the entropy. The transfer rate is defined as

$$T_{k,k'}^g = 2\text{Re} \left\{ \sum_j \int \frac{n_{j0} T_{j0}}{F_{j0}} g_{j,k}^* (k'_x k_y - k_x k'_y) [\chi_{j,k'} g_{j,k''} dz dv] \right\}. \quad (3)$$

Panels a) and b) correspond to $\omega_{T_i} = 5.5$ and 7, respectively. This cascade analysis shows that energy is depleted with each step — a conservative (inertial-range) cascade mediated by zonal-flow interactions would show constant color across k_x . Evidently, a significant amount of energy is lost inside the unstable wavenumber band. This plot is nearly identical to Fig. 1 of Ref. [10], which shows energy cascaded to stable modes. Moreover, Fig. 1 of Ref. [26], which shows the zonal-flow-catalyzed energy transfer rate to the higher- k_x stable and unstable modes in the range $0 < k_x < \sim 0.25$ at $k_y = 0.4$, indicates that the stable modes within the unstable range remove $\approx 70\%$ of the energy produced by the unstable modes. Therefore, the cascade depletion is caused by stable modes. Taken together, panels a) and b) show that energy cascade characteristics are similar in the low- and high-transport regimes, with differences primarily arising from the larger fluctuation level and broader growth rate spectrum for $\omega_{T_i} = 7$, which leads to a more robust cascade.

The zonal-flow shearing rate $\omega_s = \sum_{k_x} k_x^2 |\Phi_{ZF}|$, measured for $4.75 < \omega_{T_i} < 8$, is larger than the linear growth rate γ . The ratio $\omega_s/\gamma \approx 3$ just above the linear threshold. As the gradient

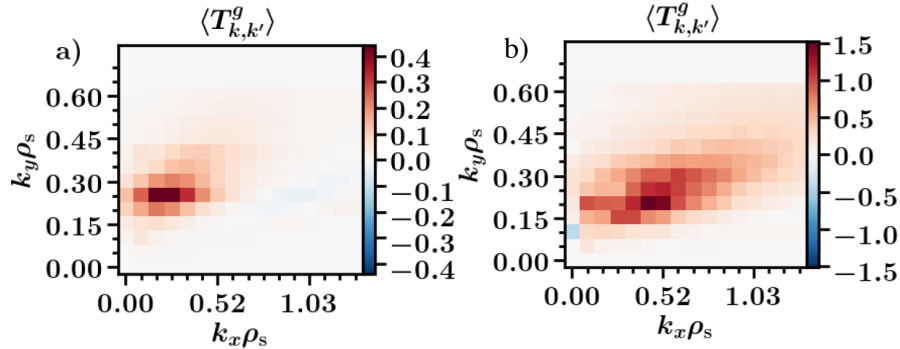


Figure 5: The time-averaged energy transfer in the zonal-flow mediated entropy cascade beginning at modes with $k_x = 0$ and different k_y to higher k_x for a) $\omega_{T_i} = 5.5$ and b) $\omega_{T_i} = 7$ at saturated state.

increases toward the NLCG the ratio slides to ~ 1.5 , and then above the NLCG jumps to > 4 . This behavior is shown in Fig. 2 of Ref. [10]. This is inconsistent with the notion that the larger fluctuation levels above the NLCG are due to a loss of efficacy of the shearing mechanism, and indicates that zonal flow shearing is not the primary arbiter of the gradient upshift.

Figs. 3–5 indicate that there is a range of strong energy removal embedded in the energy containing scales of ITG turbulence, but unlike collision-induced dissipation, energy removal is only accessed by the nonlinearity. This range of strong energy removal accounts for the well known observation that transport due to ITG turbulence is insensitive to enhanced resolution in scales beyond the unstable range. With respect to temperature gradient variation, Figs. 3–5 indicate that the energy balances that mediate saturation do not show obvious changes above the NLCG relative to below it, beyond those tied to the larger growth rates and fluctuation levels. Importantly, these figures illustrate each of the characterizations of ITG turbulence listed in Sec. 1. They show the large energy removal from stable modes at low wavenumber, the significant depletion of cascaded energy, and the role of the zonal flow in mediating energy transfer to stable modes. Critically, these features apply in both the low and high transport regimes. These results strongly suggest that zonal-flow-catalyzed transfer to stable modes mediates saturation in both regimes, and indicate that the theory previously developed for the strong-transport regime [12] should have features of the critical-gradient upshift if modified to account for the ITG instability threshold.

3 Threshold Fluid Model

We develop a fluid theory that is valid in both the low and high transport regimes. The theory is based on a reduced model for toroidal ITG turbulence that has been shown to capture the important properties of ITG turbulence discussed in the previous section [12]. This model yields solutions with strong zonal flows and provides insight about zonal-flow-catalyzed interactions, including the central idea that turbulence saturation is governed by the efficiency of energy transfer from the unstable modes to stable modes via nonlinear coupling with the zonal flow. The magnitude of the nonlinearity is determined by coupling coefficients, which quantify coupling strength between the linear eigenmodes; the eigenmode amplitudes; and the complex phases between coupled eigenmodes. The crucial complex phase for saturation is that of the cubic fluctuation correlation that governs energy transfer. With the nonlinearity described explicitly in these terms, the mechanism of turbulence saturation becomes more transparent.

The saturation theory was developed for a version of the model that does not include all necessary threshold physics associated with the onset of linear instability. As such it will not produce a reasonable description of the low and high transport regimes. Therefore, we reformulate the model to make its linear dispersion relation match that of a simplified drift-kinetic linear-instability calculation given by Hammett [29]. In the kinetic calculation, the ∇B and curvature drifts are retained in the equation for the perturbed ion distribution, yielding

$$(-i\omega + ik_{\parallel}v_{\parallel} + i\omega_{dv})\tilde{f}_i = -i \left\{ -\frac{T_i k}{eBL_n} \left[1 + \eta \left(\frac{v_{\parallel}^2}{2v_i^2} + \frac{\mu B}{v_i^2} - \frac{3}{2} \right) \right] + \omega_{dv} + k_{\parallel}v_{\parallel} \right\} \frac{e\phi}{T_i} F_{i0}, \quad (4)$$

where $\omega_{dv} = \omega_d(v_{\parallel}^2 + \mu B)/v_i^2$ is the particle-velocity-dependent magnetic drift frequency, with $\omega_d = -T_i k/(eBR)(\cos y + \hat{s}y \sin y) = -T_i k/(eBR)[1 + \mathcal{O}(y^2)]$ for $y \ll 1$. Here, y is the ballooning angle (angular distance along the field), \hat{s} is the magnetic shear, k is the poloidal wavenumber, $F_{i0} = (n_0(x)/T_{i0}(x)^{3/2}) \exp[-m(v_{\parallel}^2/2 + \mu B)/T_{i0}(x)]$ is the equilibrium distribution, e is the ion charge, R is the major radius, and $n_0(x)$ and $T_{i0}(x)$ are profiles of equilibrium density and ion temperature. Perpendicular velocity is expressed in terms of the magnetic moment $\mu = (1/2)v_{\perp}^2/B$, while $v_i = (2T_i/m_i)^{1/2}$ is the ion thermal velocity, $\eta = L_n/L_{T_i}$, and L_n and L_{T_i} are the density and

ion temperature gradient scale lengths, respectively.

The mode dispersion relation is obtained from the quasineutrality condition, $\tilde{n}_i = \tilde{n}_e$, with $\tilde{n}_e = e\phi/T_{e0}$ given by the adiabatic electron response, and $\tilde{n}_i = \int d^3v \tilde{f}_i$. Making the substitutions,

$$n_0 \frac{e\phi}{T_{e0}} = \int d^3v \frac{-\omega_{*v}^T + \omega_{dv}}{\omega - \omega_{dv}} F_{i0} \frac{e\phi}{T_{i0}}, \quad (5)$$

where, consistent with the toroidal ITG branch, we have assumed $k_{\parallel} v_{\parallel} \ll \omega, \omega_{dv}, \omega_{*v}^T$. The ion polarization contribution to the density has been neglected but will be introduced when the kinetic results are adapted to a fluid model. For ITG instability, it is possible to impose the approximation $\omega \gg \omega_{dv}$, which allows expansion of the denominator in Eq. (5) and greatly simplifies the integration. With this assumption, $(\omega - \omega_{dv})^{-1} = \omega^{-1}[1 + (\omega_{dv}/\omega) + \dots]$. Performing the velocity integrals, Eq. (5) reduces to

$$\frac{T_{i0}}{T_{e0}} = \frac{2\omega_d}{\omega} - \frac{\omega_*}{\omega} + \frac{7\omega_d^2}{\omega^2} - \frac{2\omega_d\omega_*}{\omega^2}(1 + \eta), \quad (6)$$

where $\omega_* = -T_{i0}k/(eBL_n)$. In the weak-density-gradient limit, where $\omega_* \ll \omega_*(1 + \eta), \omega_d$, solution of the quadratic dispersion relation yields

$$\omega = \left[\omega_d \pm \sqrt{\omega_d^2 - \frac{T_{i0}}{T_{e0}}(2\omega_d\bar{\omega}_{*\eta} - 7\omega_d^2)} \right] \frac{T_{e0}}{T_{i0}}, \quad (7)$$

where $\bar{\omega}_{*\eta} = \omega_*(1 + \eta)$. Instability requires that $\bar{\omega}_{*\eta}$ exceed a threshold arising from the magnetic drift frequency, i.e., $\bar{\omega}_{*\eta} > (\omega_d/2)(7 + T_{e0}/T_{i0})$. For $L_{Ti} \ll L_n$ (i.e., $\eta \gg 1$), this corresponds to a critical gradient given by $1/L_{Ti} > 1/L_{Tc} = [1/(2R)](7 + T_{e0}/T_{i0})$. Hereafter, we will assume $T_{e0}/T_{i0} = 1$.

Both the kinetic calculation and the original fluid model for the strong-transport regime [12, 17, 31] have quadratic dispersion relations. Therefore, it is possible to modify the fluid model so that it reproduces the kinetic dispersion relation. The reformulated fluid model is

$$\frac{dp_k}{dt} + \left[i\epsilon k_y (1 + \sqrt{8}) + \chi k_{\perp}^4 \right] p_k + ik_y (1 + \eta) \phi_k = - \sum_{k'} (\mathbf{k}' \hat{\mathbf{z}} \cdot \mathbf{k}) \phi_{k'} p_{k'}, \quad (8)$$

$$\begin{aligned} & [\delta(k_y) + k_{\perp}^2] \frac{d\phi_k}{dt} - 2i\epsilon k_y p_k + \left[ik_y + \nu k_{\perp}^2 + ik_y \epsilon (1 - \sqrt{8}) \right] \phi_k \\ & = \frac{1}{2} \sum_{k'} (\mathbf{k}' \times \hat{\mathbf{z}} \cdot \mathbf{k}) (k_{\perp}'^2 - k_{\perp}''^2) \phi_{k'} \phi_{k''}, \end{aligned} \quad (9)$$

where p_k and ϕ_k , respectively, are Fourier amplitudes of pressure and electrostatic potential, ν and χ are coefficients of collisional dissipation, and $\epsilon = L_n/R$. The wavenumber subscript k refers to the perpendicular wavevector \mathbf{k} , with a poloidal component k_y [denoted k in Eqs. (4)–(7)] and a radial component generated in the ballooning representation by shifts of the mode structure along the field line with respect to the outboard midplane. Aside from this shift required for the mode coupling $\mathbf{k}' \times \hat{\mathbf{z}} \cdot \mathbf{k}$, the eigenmodes are assumed to be strongly ballooning, making Eqs. (8) and (9) local in ballooning angle. The adiabatic electron response is $\delta(k_y)$, valid for all k_y , i.e., $\delta(k_y) = 0$ for $k_y = 0$, and $\delta(k_y) = 1$ for $k_y \neq 0$. In Eqs. (8) and (9), the parallel scale is normalized to L_n , and perpendicular scales are normalized to the sound gyroradius ρ_s , rendering ω_d as $k_y\epsilon$. The ion polarization drift has been included, producing $k_\perp^2 d\phi_k/dt$ and the nonlinearity in Eq. (9). The most important difference between this threshold model and prior versions in the literature [12, 17, 31] is the term $i\epsilon k_y(1 + \sqrt{8})p_k$ in the pressure equation. Absent in prior versions, it provides the correct linear instability threshold. There are other less significant variations as follows. While $T_{e0} = T_{i0}$ is assumed in all models under discussion, in Ref. [31] ν and χ are not included and the factor $(1 - \sqrt{8})$ in Eq. (9) is replaced by -2 . In Refs. [12, 17] the vorticity equation has $-i\epsilon k_y p_k$ for the pressure term, and the term $i k_y \epsilon (1 - \sqrt{8}) \phi_k$ does not appear in any form.

Consistent with a low-wavenumber regime, we assume $\chi k_\perp^2 \ll \nu$, in which case the dispersion relation is given by

$$\omega_{1,2} = \frac{1}{2(1 + k_\perp^2)} \left\{ k_y + k_y \epsilon \left[2 + (1 + \sqrt{8}) k_\perp^2 \right] - i\nu k_\perp^2 \right. \\ \left. \pm \sqrt{-8\epsilon k_y^2 (1 + \eta) (1 + k_\perp^2) + \left[-k_y + \epsilon k_y \left(4\sqrt{2} + (1 + \sqrt{8}) k_\perp^2 \right) + i\nu k_\perp^2 \right]^2} \right\}, \quad (10)$$

where \pm distinguishes the unstable and stable branches $\omega_{1,2}$. There is no assumption of weak density gradient in Eq. (10). However, we recover an exact match to Eq. (7) for $T_{e0} = T_{i0}$ in the weak-density limit. Since the L_n dependence in Eq. (10) is hidden in normalizations, its weak-density limit is readily checked by replacing $L_n \rightarrow \infty$ with $k_y \rightarrow 0$, subject to $k_y(1 + \eta) = \omega_{* \eta} \sim 1$, $\epsilon k_y = \omega_d \sim 1$, and $k_\perp^2 \ll 1$.

To use Eqs. (8) and (9) for deriving the ITG heat flux in the low and high transport regimes,

it is necessary to transform them to the eigenmode decomposition, which represents an arbitrary state p_k and ϕ_k as a finite-amplitude combination of the two linear eigenmodes, to wit,

$$\begin{pmatrix} p_k \\ \phi_k \end{pmatrix} = \beta_1(k) \begin{pmatrix} R_1(k) \\ 1 \end{pmatrix} + \beta_2(k) \begin{pmatrix} R_2(k) \\ 1 \end{pmatrix}. \quad (11)$$

Here, $[R_1(k), 1]$ and $[R_2(k), 1]$ are the eigenvectors of the unstable and stable modes, with eigenvector components R_1 and R_2 given by

$$R_{1,2}(k) = \frac{-\omega_{1,2}(1 + k_\perp^2) + k_y[1 + \epsilon(1 - \sqrt{8})] - i\nu k_\perp^2}{2k_y\epsilon}. \quad (12)$$

The eigenmode amplitudes $\beta_1(k)$ and $\beta_2(k)$ are governed by nonlinear balances consistent with the transformation of Eqs. (8) and (9) by the decomposition, Eq. (11). These equations are

$$\begin{aligned} \dot{\beta}_l + i\omega_l\beta_l &= \sum_{k', k'_y \neq 0} C_{lmn}^{(k, k')} \beta'_m \beta''_n + \sum_{k'_x} \left\{ \left[C_{lFn}^{(k, k')} v'_z \beta''_n + C_{lPn}^{(k, k')} p'_z \beta''_n \right] \Big|_{k'_y=0} \right. \\ &\quad \left. + \left[C_{lmF}^{(k, k')} \beta'_m v''_z + C_{lmP}^{(k, k')} \beta'_m p''_z \right] \Big|_{k'_y=k_y} \right\}, \end{aligned} \quad (13)$$

$$\dot{v}_z + \nu v_z = \sum_{k'} C_{Fmn}^{(k, k')} \beta''_m \beta'_n \Big|_{k_y=0}, \quad (14)$$

$$\dot{p}_z + \chi k_x^2 p_z = \sum_{k'} C_{Pmn}^{(k, k')} \beta''_m \beta'_n \Big|_{k_y=0}, \quad (15)$$

where $l, m,$ and n take the values 1 or 2, and repetition of these indices within a given term implies summation from 1 to 2, and F and P represent zonal flow and zonal pressure. Equations for the nonlinear coupling coefficients will be given below. In writing Eqs. (13)–(15), the zonal flow and zonal pressure, which are eigenmodes for $k_y = 0$, are written explicitly. A shorthand notation has been introduced for wavenumber dependence as follows: $\beta_j = \beta_j(k)|_{k_y \neq 0}$, $\beta'_j = \beta_j(k')|_{k_{y'} \neq 0}$, $\beta''_j = \beta_j(k - k')|_{k''_y \neq 0}$, $v_z = v_z(k)|_{k_y=0}$, $v'_z = v_z(k')|_{k'_y=0}$, $v''_z = v_z(k - k')|_{k''_y=k_y}$, $p_z = p_z(k)|_{k_y=0}$, $p'_z = p_z(k')|_{k'_y=0}$, and $p''_z = p_z(k - k')|_{k''_y=k_y}$, where $v_z = ik_x \phi_{k_y=0} = ik_x \phi_z$ is the zonal flow and p_z is the zonal pressure.

Figs. 2 and 3 indicate that the terms of the right-hand side of Eq. (13) with factors v'_z and v''_z dominate the nonlinearities both below and above the NLCG in the corresponding gyrokinetic system. This result can be built into Eqs. (13)–(15) by introducing an ordering scheme previously used for saturation analysis above the NLCG [12]. For that ordering a small parameter $\hat{\epsilon}$ is introduced,

and it is assumed that

$$k_y, k_\perp \sim \hat{\epsilon}^2, \quad v_z/p_z \sim \hat{\epsilon}, \quad \beta_{1,2}/\phi_z \sim \hat{\epsilon}^2. \quad (16)$$

These expressions reflect features observed in simulations, but also are rooted in physics. The first assumes that spectral energy transfer, fluctuation levels, and transport rates are dominated by long wavelengths, consistent with the large fraction of energy removed by stable modes at long wavelengths. The second is consistent with the long-wavelength assumption, given that p_z and ϕ_z are similar and $v_z \sim k_x \phi_z$. The third reflects the common observation that spectra peak at zonal wavenumbers. This is not the only ordering consistent with the dominance of the zonal-flow-catalyzed interaction, but is sufficient to produce it. When applied to Eqs. (13)–(15), the zonal pressure decouples, and the system reduces to

$$\dot{\beta}_l + i\omega_l \beta_l = \sum_{k'_x} \left\{ \left[C_{lFj}^{(k,k')} v'_z \beta'_j \right] \Big|_{k'_y=0} + \left[C_{ljF}^{(k,k')} \beta'_j v''_z \right] \Big|_{k'_y=k_y} \right\}, \quad (17)$$

$$\dot{v}_z + \nu v_z = \sum_{k'} \left[C_{Fmn}^{(k,k')} \beta''_m \beta'_n \right] \Big|_{k_y=0}, \quad (18)$$

where l , m , and n are 1 or 2, and the coupling coefficients are given by

$$C_{lFn}^{(k,k')} = \frac{(-1)^{l-1} (-ik_y)}{2(R_1(k) - R_2(k))} \left[R_n(k'') - \frac{R_{3-l}(k)[k''_\perp{}^2 - k'^2_\perp]}{1 + k'^2_\perp} \right], \quad (19)$$

$$C_{lmF}^{(k,k')} = \frac{(-1)^{l-1} (-ik'_y)}{2(R_1(k) - R_2(k))} \left[R_m(k') - \frac{R_{3-l}(k)[k''_\perp{}^2 - k'^2_\perp]}{1 + k'^2_\perp} \right], \quad (20)$$

$$C_{Fmn}^{(k,k')} = \frac{-ik'_y(k''_\perp{}^2 - k'^2_\perp)}{2}. \quad (21)$$

Equations (17) and (18) represent an energy-conserving reduction of the larger set of nonlinear interactions present in Eqs. (13)–(15). Consequently, these equations, which isolate zonal-flow-catalyzed transfer to the stable mode, give a realistic model of the physics that dominates saturation and transport in the ITG-driven system under investigation. The coupling coefficients of Eqs. (19) and (20) combine the two nonlinearities of Eqs. (8) and (9). The first term in the square brackets represents the pressure nonlinearity of Eq. (8) and the second the vorticity nonlinearity of Eq. (9).

4 Relationships between Turbulent Correlations

The ion heat flux is given by $Q_i = -\sum_k k_y \text{Im}\langle\phi_{-k} p_k\rangle$, requiring a solution for the nonlinear correlation $\langle\phi_{-k} p_k\rangle$ consistent with steady state solutions of Eqs. (17) and (18). The first step is to render the flux in the eigenmode decomposition by substituting from Eq. (11), yielding

$$Q_i = -\sum_k k_y \left[\text{Im}R_1 |\beta_1|^2 + \text{Im}R_2 |\beta_2|^2 + \text{Im}(R_1 + R_2) \text{Re}\langle\beta_1 \beta_2^*\rangle + \text{Re}(R_1 - R_2) \text{Im}\langle\beta_1 \beta_2^*\rangle \right]. \quad (22)$$

Noting that $\text{Im}R_1$ is proportional to γ , the first term is essentially the quasilinear flux, assuming $|\beta_1|^2$ is supplied from a nonlinear simulation or a measurement. The remaining terms, which arise because of the nonlinear excitation of the stable mode, require solution for $|\beta_2|^2$ and $\langle\beta_1 \beta_2^*\rangle$. There are also parametric dependencies in $|\beta_1|^2$ that can be missed in quasilinear theory and will be treated here, as well. Missed dependencies are illustrated by nonlinear finite- β electromagnetic stabilization, where the ITG heat flux decreases with β more strongly than the growth rate [32, 38]. The parameter β is the plasma pressure normalized by the magnetic pressure. This can be explained in part by an important scaling of $|\beta_1|^2$ with β arising from the nonlinear correlation time that mediates saturation [26, 33]. In the modeling of Refs. [26, 33], contributions to the heat flux from $|\beta_2|^2$ and $\langle\beta_1 \beta_2^*\rangle$ were neglected. Here, they are retained and calculated to formulate a description of the critical-gradient upshift.

In saturation, $|\beta_j|^2$ and $\langle\beta_1 \beta_2^*\rangle$ can be evaluated from energy evolution equations of statistical closure theory, as done in Ref. [12]. These equations are linearized when energy transfer is dominated by the interaction of unstable mode, stable mode, and zonal flow. The equations have robust parameter scalings, but their solution requires the inversion of a large matrix, and interpretation of individual roots is difficult. Here we utilize an approach based on nonlinear conservation properties and the nearly conjugate symmetry of unstable and stable modes for small ν . Conjugate symmetry carries over to the nonlinear couplings in the eigenmode decomposition, as seen in Eqs. (19) and (20). These symmetries produce relationships between $|\beta_2|^2$, $\langle\beta_1 \beta_2^*\rangle$, and $|\beta_1|^2$ that for low collisionality, small wavenumber, and steady state are governed by linear physics. As a result, Eq. (22) can be expressed solely in terms of $|\beta_1|^2$. We derive these relationships in this section and solve a

nonlinear balance for $|\beta_1|^2$ in Sec. 5.

We first consider the complex correlation $\langle \beta_1 \beta_2^* \rangle$ and the physics of its cross phase, which have received limited attention. For turbulence governed by Eqs. (17) and (18), the phase is dominated by linear physics. Consider summing Eq. (17) over $l = 1, 2$, yielding

$$\begin{aligned} \dot{\beta}_1 + \dot{\beta}_2 + i\omega_1\beta_1 + i\omega_2\beta_2 &= \sum_{k'_x} \left[\left(C_{1F1}^{(k,k')} + C_{2F1}^{(k,k')} \right) \beta_1'' + \left(C_{1F2}^{(k,k')} + C_{2F2}^{(k,k')} \right) \beta_2'' \right] v'_z \Big|_{k'_y=0} \\ &+ \sum_{k'_x} \left[\left(C_{11F}^{(k,k')} + C_{21F}^{(k,k')} \right) \beta_1' + \left(C_{12F}^{(k,k')} + C_{22F}^{(k,k')} \right) \beta_2' \right] v'_z \Big|_{k'_y=k_y}. \end{aligned} \quad (23)$$

From Eqs. (19) and (20), it is readily found that

$$C_{1F1}^{(k,k')} + C_{2F1}^{(k,k')} = C_{1F2}^{(k,k')} + C_{2F2}^{(k,k')} = \frac{-ik_y}{2(1+k_\perp^2)} (k''_\perp{}^2 - k'_\perp{}^2), \quad (24)$$

$$C_{11F}^{(k,k')} + C_{21F}^{(k,k')} = C_{12F}^{(k,k')} + C_{22F}^{(k,k')} = \frac{-ik'_y}{2(1+k_\perp^2)} (k''_\perp{}^2 - k'_\perp{}^2). \quad (25)$$

In Eqs. (24) and (25), the pressure nonlinearity contributions cancel out, while the vorticity nonlinearity contributions add, generating the rightmost expressions. The cancellation occurs because energy removed from the unstable mode through the zonal flow by the pressure nonlinearity is deposited in total into the stable mode. On the other hand, the vorticity nonlinearity removes energy from both modes and deposits it into the zonal flow. It therefore does not cancel in a sum involving $\dot{\beta}_1$ and $\dot{\beta}_2$.

The vorticity nonlinearity is smaller than the pressure nonlinearity by a factor k_\perp^2 . This is quantified under the ordering that describes the saturation energetics, $C_{lFn} \sim C_{lmF} \sim k \sim \hat{\epsilon}^2$ and $C_{Flm} \sim \hat{\epsilon}^6$, where $\hat{\epsilon}$ is the small ordering parameter. Because the pressure nonlinearity cancels in Eqs. (24) and (25),

$$\dot{\beta}_1 + \dot{\beta}_2 + i\omega_1\beta_1 + i\omega_2\beta_2 = \mathcal{O}(\hat{\epsilon}^6) \cdot v'_z \beta_n''. \quad (26)$$

The saturated value of v'_z is order unity, hence the right-hand side of Eq. (26) is much smaller than the left-hand side. Consequently, the cross phase of $\langle \beta_1 \beta_2^* \rangle$, which can be constructed from the left-hand side of Eq. (26), is dominated by linear physics.

Equation (26) indicates that, in the steady state, there is a fixed relation between β_1 and β_2 . Accordingly, we adopt the ansatz $\beta_2 = \sqrt{\kappa} \exp(i\theta) \beta_1$, where the saturated mode amplitude ratio

$\kappa \equiv |\beta_2|^2 / |\beta_1|^2$ will be determined from a separate relationship that will be introduced shortly. Substituting $\beta_2 = \sqrt{\kappa} \exp(i\theta)\beta_1$ into Eq. (26), with the right-hand side set to zero, we obtain

$$\left(1 + \sqrt{\kappa}e^{i\theta}\right) \dot{\beta}_1 + i\left(\omega_1 + \omega_2\sqrt{\kappa}e^{i\theta}\right) \beta_1 = 0 . \quad (27)$$

We multiply Eq. (27) by β_1^* and sum it with its conjugate equation, obtaining

$$\left|\dot{\beta}_1\right|^2 - 2\text{Im}\left(\frac{\omega_1 + \omega_2\sqrt{\kappa}e^{i\theta}}{1 + \sqrt{\kappa}e^{i\theta}}\right) |\beta_1|^2 = 0 . \quad (28)$$

This is not an equation for $|\beta_1|^2$ or its evolution, because those require a nonlinear balance. Rather, it is an equation for θ consistent with Eq. (26). Having been constructed at the level of squared amplitudes, the imposition of a steady-state condition $|\dot{\beta}_1|^2 = 0$ represents the average of an energy-like quantity with the random phase of the raw amplitude β_1 removed. The stationary condition, aside from the trivial solution $|\beta_1|^2 = 0$, requires

$$\text{Im}\left(\frac{\omega_1 + \omega_2\sqrt{\kappa}e^{i\theta}}{1 + \sqrt{\kappa}e^{i\theta}}\right) = 0 , \quad (29)$$

which is the desired expression that sets the value of θ . Rationalizing the denominator, Eq. (29) implies that

$$\text{Im}\left[\left(\omega_1 + \omega_2\sqrt{\kappa}e^{i\theta}\right)\left(1 + \sqrt{\kappa}e^{-i\theta}\right)\right] = \text{Im}\left[\omega_1 + \omega_1\sqrt{\kappa}e^{-i\theta} + \omega_2\kappa + \omega_2\sqrt{\kappa}e^{i\theta}\right] = 0 . \quad (30)$$

To collect the θ dependence in a single term, we introduce the frequency difference $\Delta\omega = \omega_2 - \omega_1^*$ and write the two ω_2 -dependent terms in the right-hand part of the above expression in terms of $\Delta\omega$. Solving the resulting expression for θ yields

$$\theta = -\tan^{-1}\left(\frac{\text{Im}(\Delta\omega)}{\text{Re}(\Delta\omega)}\right) + \sin^{-1}\left[\frac{\text{Im}(\omega_1^* - \omega_2\kappa)}{\sqrt{\kappa}|\omega_2 - \omega_1^*|}\right] , \quad (31)$$

As previously stated, this expression supplies the angle θ in the correlations $\langle\beta_1\beta_2^*\rangle = \sqrt{\kappa}|\beta_1|^2 \exp(-i\theta)$, $\text{Re}\langle\beta_1\beta_2^*\rangle = \sqrt{\kappa}|\beta_1|^2 \cos\theta$, and $\text{Im}\langle\beta_1\beta_2^*\rangle = -\sqrt{\kappa}|\beta_1|^2 \sin\theta$ that appear in Eq. (22).

The factor κ is a ratio of saturation levels. The levels for $|\beta_1|^2$ and $|\beta_2|^2$ individually depend on nonlinear balances. However, the similarity properties of nonlinear transfer associated with energy conservation suggest that the nonlinear transfer rates in equations for $|\beta_1|^2$ and $|\beta_2|^2$ are

very similar. The ratio of $|\beta_1|^2$ and $|\beta_2|^2$ would then be governed by the ratio of rates of energy injection and removal. This is an observed feature in gyrokinetic simulations, where there are many stable modes [24]. For the conditions of Ref. [24], the energy damping rate of each stable mode is approximately equal for the 1200 modes with smallest damping rates, and their sum balances the energy injection rate. These rates are given by $\gamma_j|\beta_j|^2$. We revisit the tendency of equipartition of these rates for the present simpler system, formulating it from the properties of the equations instead of measuring it as an aspect of a simulation.

We assess the energy rates $\gamma_j|\beta_j|^2$ from the energy itself, which is given by

$$E = \sum_{k_y \neq 0} \left[\left(1 + k_\perp^2 + |R_1|^2\right) |\beta_1|^2 + \left(1 + k_\perp^2 + |R_2|^2\right) |\beta_2|^2 \right. \\ \left. + 2 \left(1 + k_\perp^2\right) \text{Re}\langle\beta_1^*\beta_2\rangle + 2\text{Re}\langle R_1^*\beta_1^*R_2\beta_2\rangle \right] + \sum_{k_y=0} \left[|p_k|^2 + k_\perp^2 |\phi_k|^2 \right]. \quad (32)$$

Because the nonlinear interactions of Eqs. (17) and (18) are conservative, dE/dt is governed solely by dissipative terms, i.e., the nonlinearities associated with time derivatives of $|\beta_j|^2$ and $\langle\beta_1^*\beta_2\rangle$ cancel each other. In steady state, dE/dt then describes the balance of energy injection and removal according to

$$\frac{dE}{dt} = \sum_{k_y \neq 0} \left\{ 2\text{Im}(\omega_1) \left(1 + |R_1|^2 + k_\perp^2\right) |\beta_1|^2 + 2\text{Im}(\omega_2) \left(1 + |R_2|^2 + k_\perp^2\right) |\beta_2|^2 \right. \\ \left. + 2 \left(1 + k_\perp^2\right) \text{Im} \left[(\omega_1^* - \omega_2) \langle\beta_1^*\beta_2\rangle \right] + 2\text{Im} \left[R_1^*R_2 (\omega_1^* - \omega_2) \langle\beta_1^*\beta_2\rangle \right] \right\} \\ - 2\nu \sum_{k_x} |v_z|^2 \Big|_{k_y=0} = 0. \quad (33)$$

We first examine Eq. (33) in the collisionless limit, $\nu = 0$, where $\omega_1^* - \omega_2 = 0$ and $|R_1|^2 = |R_2|^2$. In this limit, we find that

$$\frac{dE}{dt} = \sum_{k_y \neq 0} \left[2\text{Im}(\omega_1) \left(1 + |R_1|^2 + k_\perp^2\right) |\beta_1|^2 + 2\text{Im}(\omega_2) \left(1 + |R_2|^2 + k_\perp^2\right) |\beta_2|^2 \right] \\ = \sum_{k_y \neq 0} \left[2\text{Im}(\omega_1) \left(1 + |R_1|^2 + k_\perp^2\right) \left(|\beta_1|^2 - |\beta_2|^2 \right) \right] = 0, \quad (34)$$

i.e., the energy injected into turbulence by the unstable modes is removed totally by the stable mode. With $\gamma_1 = -\gamma_2$, this implies $|\beta_1(k)|^2 = |\beta_2(k)|^2$. This is a reflection of the complex-conjugate symmetry of the two eigenmodes when $\nu = 0$.

The collisionless limit is not strictly applicable for saturation with Eqs. (17) and (18), because collisionality balances the inverse energy transfer of the vorticity nonlinearity in Eq. (18). This gives rise to the last term of Eq. (33). We are nonetheless interested in the limit of small collisionality, noting that $\nu \neq 0$ makes $\omega_1^* \neq \omega_2$, $R_1^* \neq R_2$, and $|\beta_1|^2 \neq |\beta_2|^2$. To examine the effects of small collisionality on the ratio $\kappa = |\beta_2|^2/|\beta_1|^2$, we introduce ν into the ordering of Eq. (16) as $\nu \sim k^2 \sim \hat{\epsilon}^4$. Under this extended ordering, we return to Eq. (33) and examine each term. We note that k_\perp^2 does not break conjugate symmetry, i.e., for $\nu = 0$, the equality $\omega_1^* = \omega_2$ holds with terms of order k_\perp^2 included. However, ν itself is multiplied by k_\perp^2 in ω_j and R_j , raising the order of the symmetry-breaking contributions in the first four terms of Eq. (33). The last term requires special consideration, as discussed below.

From Eq. (10), we find that $\omega_1^* = \omega_2 + \mathcal{O}(\nu k_\perp^2) = \omega_2 + \mathcal{O}(\hat{\epsilon}^6)$, i.e., the first deviation of ω_2 from ω_1^* occurs at sixth order. From Eq. (12), we note that the breaking of conjugate symmetry in R_j resides in the term proportional to ω_j . Hence, $R_1^* = R_2 + \mathcal{O}(\nu k_\perp^2)$. The terms of Eq. (33) with dependence on the cross-correlation $\langle \beta_1^* \beta_2 \rangle$ have a factor $\omega_1^* - \omega_2$ and are therefore $\mathcal{O}(\nu k_\perp^2)$. The last term of Eq. (33) is proportional to $|v_z|^2$, hence its magnitude requires knowledge of saturation levels. The levels of $|\beta_1|^2$ and $|v_z|^2$ are given in Ref. [12] in terms of basic scalings, and are sufficient to estimate the order of the term $\nu |v_z|^2$ in Eq. (33). From Eqs. (33) and (40) of Ref. [12],

$$|v_z|^2 = \frac{2\gamma_1}{\nu b} \frac{|C_{F12}|}{|C_{1F2}|} |\beta_1|^2, \quad (35)$$

where b is a constant of order unity in the $\hat{\epsilon}$ expansion.

With this expression, Eq. (33) can be written

$$2 \sum_{k_y \neq 0} |\beta_1|^2 \gamma_1 \left(1 + k_\perp^2 + |R_1|^2 - \frac{|C_{F12}|}{b|C_{1F2}|} \right) = 2 \sum_{k_y \neq 0} |\beta_2|^2 |\gamma_2| (1 + k_\perp^2 + |R_2|^2) + \mathcal{O}(\nu k_\perp^2), \quad (36)$$

where the contributions of $\mathcal{O}(\nu k_\perp^2)$ represent the terms proportional to $\langle \beta_1^* \beta_2 \rangle$. From this expression, we obtain

$$\kappa = \frac{|\beta_2(k)|^2}{|\beta_1(k)|^2} = \frac{\gamma_1 \left(1 + |R_1|^2 + k_\perp^2 - \frac{|C_{F12}|}{b|C_{1F2}|} \right)}{|\gamma_2| (1 + |R_2|^2 + k_\perp^2)} + \frac{\mathcal{O}(\nu k_\perp^2)}{|\gamma_2| (1 + |R_2|^2 + k_\perp^2)}, \quad (37)$$

where, in keeping with the strong localization of dominant energy transfer in the low wavenumber range, we have replaced the sum with evaluation at a representative wavenumber.

We now examine the order of the leading contribution to $|R_j|^2$, which from Eq. (12) is $-\omega_j(1+k_\perp^2)/(2k_y\epsilon) \sim \mp\sqrt{(1+\eta)\epsilon}$. Following Eq. (10) we compare the threshold dispersion relation to the results of Ref. [29], which assumes a flat density limit $L_n \rightarrow \infty$, and which was ordered as $(1+\eta)k_y \sim \mathcal{O}(1)$ and $\epsilon k_y \sim \mathcal{O}(1)$. The more appropriate limit is for a modestly peaked density profile with $\mathcal{O}(\hat{\epsilon}^2) \leq \epsilon < \mathcal{O}(1)$. Because $R_2|^2 = |R_1|^2 + \mathcal{O}(\nu^2 k_\perp^4)$, Eq. (37) can then be written

$$\kappa = \frac{\gamma_1}{|\gamma_2|} \left(1 - \frac{|C_{F12}|}{b|R_1|^2|C_{1F2}|} \right) + \frac{\mathcal{O}(\nu k_\perp^2)}{|\gamma_2| |R_1|^2}, \quad (38)$$

where for $\epsilon = \mathcal{O}(\hat{\epsilon}^2)$, this expression is valid to eighth order, and $\gamma_1/|\gamma_2|$ differs from unity in the sixth order.

The above analysis shows that equipartition of energy rates $\gamma_j|\beta_j|^2$ is followed to high order in this system, with small deviations arising from the breaking of conjugate symmetry in γ_1 and γ_2 by finite collisionality. The result is that κ deviates from unity by a small increment of order νk_\perp^2 .

With these results, we return to the heat flux in Eq. (22), and write it up to order $\nu k_\perp^2 \sim \hat{\epsilon}^6$, yielding

$$Q_i = \sum_k \frac{\gamma_1}{2\epsilon} (1 + k_\perp^2) |\beta_1|^2 (1 - \kappa). \quad (39)$$

This equation provides three pieces of important information. First, the heat flux is proportional to the growth rate of the instability, a standard result for drift-wave turbulence [34]. Second, the heat flux is proportional to the turbulence level. While this is also standard, the turbulence level is set by a saturation balance, which introduces dependencies on coupling coefficients and the triplet correlation time, with their tendency for resonance in a wave regime at low k . These dependencies are derived in the Sec. 5. The third important concept is that the heat flux is proportional to $1 - \kappa$, arising from $\text{Im}(R_1)|\beta_2|^2 + \text{Im}(R_2)|\beta_2|^2$. The high degree of conjugate symmetry for weakly collisional regimes puts the stable-mode amplitude on par with that of the unstable mode, significantly reducing the heat flux.

5 Nonlinear Saturation Relations

We turn now to the nonlinear physics that sets $|\beta_1|^2$. The level $|\beta_1|^2$ is governed by a saturation energy balance that depends on the triplet correlation time τ of the fluctuation interaction that

mediates saturation. The triplet correlation time of interest in the present, zonal-flow-mediated case is essentially the reciprocal of the frequencies of the unstable mode, the zonal flow, and the stable mode, each at a wavenumber of the triplet interaction $k = k' + k''$. More precisely we write $\tau = -i[\omega_l(k'') + \omega_m(k') - \omega_n^*]^{-1}$, where l , m , and n respectively denote stable mode, zonal flow, and unstable mode. These frequencies have linear and nonlinear components, with the former given by Eq. (10). When the triplet correlation time is near resonance, the sum of the linear frequencies nearly vanishes, and the nonlinear frequencies become important. Hence, we also derive the nonlinear frequency, or eddy damping rate, as a function of turbulence levels. Both of these relationships are obtained from statistical closure theory. The statistical closure theory for Eqs. (17) and (18) was worked out in Ref. [12]. While that derivation was restricted to the strong-transport regime, it used the form and symbols of Eqs. (17)–(21) — one only need supply the correct threshold-model expressions for $R_{1,2}$ from Eq. (12) and $\omega_{1,2}$ from Eq. (10).

Statistical closure treats the nonlinear terms of energy evolution equations. For the zonal flow, the energy evolution equation is obtained from Eq. (18) and given by

$$|\dot{v}_z|^2 + \nu|v_z|^2 = 2\text{Re} \sum_{k'} C_{Fmn}^{(k,k')} \langle \beta''_m \beta'_n v_z^* \rangle \Big|_{k_y=0}, \quad (40)$$

where n and m can take the values of 1 or 2, and repetition of these indices in any single term indicates a sum from 1 to 2. The triplet correlation $\langle \beta''_m \beta'_n v_z^* \rangle$ governs nonlinear transfer, and it is calculated from its evolution equation, which from Eqs. (17) and (18) is given by

$$\begin{aligned} & \left[\frac{d}{dt} + i\omega''_m + i\omega'_n - i\omega_1^* \right] \langle \beta''_m \beta'_n v_z^* \rangle \Big|_{k_y=0} = \\ & \sum_{k''_x} \left\{ \left[C_{mFl}^{(k'',k''')} \langle v_z''' \beta_l(k'' - k''') \beta'_n v_z^* \rangle + C_{nFl}^{(k',k''')} \langle v_z''' \beta_l(k' - k''') \beta''_m v_z^* \rangle \right] \Big|_{k''_y=0} + \right. \\ & \left. \left[C_{mlF}^{(k'',k''')} \langle \beta_l''' v_z(k'' - k''') \beta'_n v_z^* \rangle \Big|_{k''_y=k''_y} + C_{nlF}^{(k',k''')} \langle \beta_l''' v_z(k' - k''') \beta''_m v_z^* \rangle \Big|_{k''_y=k''_y} \right] \right\} \Big|_{k_y=0}, \quad (41) \end{aligned}$$

where the nonlinearity that drives v_z^* has been neglected because it is smaller by a factor of k_\perp^2 than the nonlinearities of the right-hand side that drive β''_m and β'_n .

Equation (41) is inverted and substituted into Eq. (40). The fourth-order correlations of Eq. (41) are written as products of two second-order correlations, i.e., $\langle v_z''' \beta_l(k'' - k''') \beta'_n v_z^* \rangle \rightarrow$

$\langle \beta_l'^* \beta_n' \rangle |v_z|^2$, $\langle v_z''' \beta_l(k' - k''') \beta_m'' v_z^* \rangle \rightarrow \langle \beta_l''^* \beta_m'' \rangle |v_z|^2$, $\langle \beta_l''' v_z(k'' - k''') \beta_n' v_z^* \rangle \rightarrow \langle \beta_l''^* \beta_n' \rangle |v_z|^2$, and $\langle \beta_l''' v_z(k' - k''') \beta_m'' v_z^* \rangle \rightarrow \langle \beta_l''^* \beta_m'' \rangle |v_z|^2$. Writing fourth-order correlations as products of second-order correlations assumes turbulence with a probability distribution function that is close to a Gaussian, which is valid for a randomized system, in which case the sum over k_x''' is dominated by $k_x''' = k_x$ in the first and second terms on the right-hand side of Eq. (41), by $k_x''' = k_x'' - k_x$ in the third, and by $k_x''' = k_x' - k_x$ in the fourth.

The interaction of β_m'' , β_n' , and v_z^* has a finite correlation time governed by the frequency mismatch $i\omega_m'' + i\omega_n' - i\omega_1^*$. In a steady state, $\langle \beta_m'' \beta_n' v_z^* \rangle$ is given by the right-hand side of Eq. (41) divided by $i\omega_m'' + i\omega_n' - i\omega_1^*$. This means that $\langle \beta_m'' \beta_n' v_z^* \rangle$ tends to be dominated by mode interactions for which $i\omega_m'' + i\omega_n' - i\omega_1^*$ is minimal. Moreover, such interactions result in lower values of fluctuation levels for a given linear drive. Physically, $i\omega_m'' + i\omega_n' - i\omega_1^*$ is the reciprocal of the triplet correlation time; when this time is large, energy transfer is more efficient, and the system saturates at lower turbulent amplitudes.

Consider couplings that make $i\omega_m'' + i\omega_n' - i\omega_1^*$ minimal. By assignment, k is the wavenumber of the zonal flow, which we assume is a zero-frequency fluctuation with damping that is very small ($\nu \ll 1$). Then, if $m = 1$, a minimum occurs for $n = 2$, i.e., $|i\omega_1'' + i\omega_2' - i\omega_1^*| \ll |i\omega_1'' + i\omega_1' - i\omega_1^*|$. Similarly, for $m = 2$, a minimum occurs for $n = 1$, and $|i\omega_2'' + i\omega_1' - i\omega_1^*| \ll |i\omega_2'' + i\omega_2' - i\omega_1^*|$. This property follows from the near-conjugate symmetry of the unstable and stable modes. It also validates the assertion made in Sec. 1 that the nonlinear coupling is dominated by the interaction of the unstable mode, the zonal flow, and the stable mode. It is worth noting that if $\nu = k_\perp^2 = 0$, $|i\omega_1'' + i\omega_2' - i\omega_1^*|$ and $|i\omega_2'' + i\omega_1' - i\omega_1^*|$ exactly vanish. This makes nonlinear frequencies important even in a weak-turbulence regime where the nonlinear frequency at a single k is small compared to its linear counterpart. Restricting three-wave coupling to the interaction of the unstable mode,

zonal flow, and stable mode, the closed equation for $|v_z|^2$ is given by

$$\begin{aligned}
\left[\frac{\partial}{\partial t} + 2\nu \right] |v_z|^2 \Big|_{k_y=0} &= \sum_{k'} 2\text{Re} \left\{ C_{F12}^{(k,k')} (i\omega'_2 + i\omega''_1 - i\omega_1^*)^{-1} |v_z|^2 \left[\left(C_{22F}^{(k',-k'')} + C_{2F2}^{(k',k)} \right) \langle \beta_1'' \beta_2''^* \rangle \right. \right. \\
&+ \left. \left(C_{1F1}^{(k'',k)} + C_{11F}^{(k'',-k')} \right) \langle \beta_1' \beta_2' \rangle + \left(C_{1F2}^{(k'',k)} + C_{12F}^{(k'',-k')} \right) |\beta_2'|^2 + \left(C_{21F}^{(k',-k'')} + C_{2F1}^{(k',k)} \right) |\beta_1''|^2 \right] \\
&+ C_{F21}^{(k,k')} (i\omega''_2 + i\omega'_1 - i\omega_1^*)^{-1} |v_z|^2 \left[\left(C_{21F}^{(k',-k'')} + C_{1F1}^{(k',k)} \right) \langle \beta_1''^* \beta_2'' \rangle + \left(C_{12F}^{(k',-k'')} + C_{1F2}^{(k',k)} \right) |\beta_2''|^2 \right. \\
&\left. \left. + \left(C_{2F1}^{(k'',k)} + C_{21F}^{(k'',-k')} \right) |\beta_1'|^2 + \left(C_{2F2}^{(k'',k)} + C_{22F}^{(k'',-k')} \right) \langle \beta_1' \beta_2'^* \rangle \right] \right\} \Big|_{k_y=0}. \quad (42)
\end{aligned}$$

Here, the notion of steady state that allows inversion of Eq. (41) with $(i\omega'_2 + i\omega''_1 - i\omega_1^*)^{-1}$ is, in fact, the Markovian assumption of the eddy-damped-quasi-normal-Markovian closure, commonly referred to as EDQNM [35], valid when the time scales of fluctuation correlations is slower than $(i\omega'_2 + i\omega''_1 - i\omega_1^*)^{-1}$. In Sec. 6, we will solve this equation to obtain the saturated level of $|\beta_1|^2$ pursuant to an analytic expression for the heat flux.

As constructed in Eq. (41), the triplet correlation times $(i\omega'_2 + i\omega''_1 - i\omega_1^*)^{-1}$ and $(i\omega''_2 + i\omega'_1 - i\omega_1^*)^{-1}$ are made up of linear frequencies. However, in turbulent systems, any linear frequency has a nonlinear counterpart that describes the effect of nonlinear scattering on wave properties. These nonlinear frequencies are often referred to as eddy damping, because they lead to decorrelation at an amplitude-dependent rate. In turbulence with wave motion, these frequencies are complex, just like linear frequencies. As shown in Ref. [36], eddy damping arises from nonlinear interactions that are separate from those that converted the fourth-order correlations of Eq. (41) to products of second-order correlations, and the eddy damping can be formulated from those interactions [36].

We derive the complex eddy damping rate that renormalizes the linear frequency ω_l . Starting from Eq. (17), we observe that the nonlinearity involves products $v'_z \beta_j''$ and $\beta_j' v''_z$. Such products themselves satisfy a nonlinear evolution equation, which for $v'_z \beta_j''$ is constructed from Eqs. (17) and (18) and given by

$$\begin{aligned}
\left[\frac{d}{dt} + i\omega''_j + i\omega'_1 \right] \beta_j'' v'_z \Big|_{k'_y=0} &= \sum_{k''} \left\{ C_{jFl}^{(k'',k''')} v_z''' \beta_l(k'' - k''') v'_z \Big|_{k''_y, k'_y=0} \right. \\
&+ \left. C_{j'lF}^{(k'',k''')} v_z(k'' - k''') \beta_l''' v'_z \Big|_{k''_y=k'_y, k'_y=0} + C_{Fml}^{(k',k''')} \beta_m''' \beta_l(k' - k''') \beta_j'' \Big|_{k'_y=0} \right\}. \quad (43)
\end{aligned}$$

To find contributions to the eddy-damping counterpart of ω_l from the sum over k_x''' , we select wavenumbers that give the right-hand side of Eq. (43) the same phase as β_l . For the first term of the right-hand side of Eq. (43) this is accomplished with $k_x''' = -k_x'$, for the second term with $k_x''' = 0$, and for the third term with $k_x''' = k_x$ and $k_x''' = k_x' - k_x$. Consequently, in steady state, Eq. (43) becomes

$$v_z' \beta_j'' \Big|_{k_y'=0} = \frac{1}{i(\omega_j'' + \omega_1')} \left\{ \left(C_{jFl}^{(k'',-k')} + C_{jLF}^{(k'',k)} \right) |v_z'|^2 + \sum_m \left[C_{Flm}^{(k',k)} \beta_m'' \beta_j'' + C_{Fml}^{(k',-k'')} \beta_m'' \beta_j'' \right] \right\} \Big|_{k_y'=0} \beta_l. \quad (44)$$

We observe that, although the right-hand side of Eq. (44) is nonlinear, its phase is that of β_l , because $|v_z'|^2$ and $\beta_m'' \beta_j''$ have zero phase for $m = j$, and for $m \neq j$ the phase is very small as seen from Eq. (31). Applying the procedure that produced Eq. (44) to $\beta_j' v_z''$, we obtain

$$v_z'' \beta_j'' \Big|_{k_y'=k_y} = \frac{1}{i(\omega_j'' + \omega_1'')} \left\{ \left(C_{jFl}^{(k',-k'')} + C_{jLF}^{(k',k)} \right) |v_z''|^2 + \sum_m \left[C_{Flm}^{(k'',k)} \beta_m' \beta_j' + C_{Fml}^{(k'',-k')} \beta_m' \beta_j' \right] \right\} \Big|_{k_y'=k_y} \beta_l. \quad (45)$$

When these two expressions are substituted into Eq. (17) the factors multiplying β_l combine to produce an eddy turnover rate given by

$$\Delta\omega_l = 2 \sum_{k_x'} \frac{C_{lFj}^{(k,k')}}{i(\hat{\omega}_j'' + \hat{\omega}_1')} \left[\left(C_{jFl}^{(k'',-k')} + C_{jLF}^{(k'',k)} \right) |v_z'|^2 + \left(C_{Flm}^{(k',k)} + C_{Fml}^{(k',-k'')} \right) \beta_m'' \beta_j'' \right], \quad (46)$$

where the full frequency of β_l is written $i\hat{\omega}_l = i\omega_l - \Delta\omega_l$, and we note that the frequencies inside $\Delta\omega_l$ are themselves renormalized by eddy damping rates. The latter renormalization guarantees that $\hat{\omega}_l$ has low and high transport regimes, consistent with the observations depicted in Fig. 9 of Ref. [37].

While the eddy damping rate must have dimensions of the reciprocal of time and depend on amplitude, there is some ambiguity regarding the form of the nonlinear damping time $[i(\hat{\omega}_j' + \hat{\omega}_1'')]^{-1}$ in Eq. (46). For example, in Ref. [36] this time is the same as the nonlinear time that governs the three-wave interactions of the energy evolution equations. This puts three frequencies in the nonlinear damping time of $\Delta\omega_l$ as given in Eq. (2) of Ref. [10]. As derived here, $\Delta\omega_l$ is the scattering

rate associated with the frequency of a single-mode, three of which then enter the triplet correlation time. The single mode damping time has been measured in simulation and compared with analytic forms [37].

6 Heat Flux Solutions

To evaluate the nonlinear expression for heat flux in Eq. (22) we solve the zonal energy balance Eq. (42) for $|\beta_1|^2$, first simplifying its form. Consider the four terms of Eq. (42) whose spectral correlations are functions of k'' . We exchange the wavenumbers k' and k'' , which are assigned arbitrarily in the convolution generated by the Fourier transform of the nonlinearity. With the exception of the factors $C_{F12}^{(k,k'')}$ and $C_{F21}^{(k,k'')}$, this operation maps terms of Eq. (42) whose spectral correlations are functions of k'' into the terms whose spectral correlations are functions of k' . We then note that for $k_y = 0$, we have $C_{F12}^{(k,k'')} = C_{F21}^{(k,k')} = C_{F12}^{(k,k')} = C_{F21}^{(k,k'')}$, a property that can be readily verified from Eq. (21). Consequently, Eq. (42) becomes

$$\begin{aligned} \left[\frac{\partial}{\partial t} + 2\nu \right] |v_z|^2 \Big|_{k_y=0} &= 4 \sum_{k'} \text{Re} \left\{ C_{F12}^{(k,k'')} \tau_{12F} \left[\left(C_{1F1}^{(k'',k)} + C_{11F}^{(k'',-k')} \right) \langle \beta_1^* \beta_2' \rangle \right. \right. \\ &\quad \left. \left. + \left(C_{1F2}^{(k'',k)} + C_{12F}^{(k'',-k')} \right) |\beta_2'|^2 \right] + C_{F21}^{(k,k'')} \tau_{21F} \left[\left(C_{2F2}^{(k'',k)} + C_{22F}^{(k'',-k')} \right) \right. \right. \\ &\quad \left. \left. \times \langle \beta_1' \beta_2^* \rangle + \left(C_{2F1}^{(k'',k)} + C_{21F}^{(k'',-k')} \right) |\beta_1'|^2 \right] \right\} |v_z|^2 \Big|_{k_y=0}, \end{aligned} \quad (47)$$

where $\tau_{21F} = (i\hat{\omega}_2'' + i\hat{\omega}_1' - i\hat{\omega}_1^*)^{-1}$ and $\tau_{12F} = (i\hat{\omega}_1'' + i\hat{\omega}_2' - i\hat{\omega}_1^*)^{-1}$ are the triplet correlation times for the zonal-flow-catalyzed triplet interaction. Defining amalgamated coefficients $C''_{mn} = C_{mFn}^{(k'',k)} + C_{mnF}^{(k'',-k')}$, the spectral balance acquires the succinct form

$$\begin{aligned} \left[\frac{\partial}{\partial t} + 2\nu \right] |v_z|^2 \Big|_{k_y=0} &= 4 \sum_{k'} \text{Re} \left\{ \left[C_{F12}^{(k,k'')} \tau_{12F} \left(C''_{11} \langle \beta_1^* \beta_2' \rangle + C''_{12} |\beta_2'|^2 \right) \right. \right. \\ &\quad \left. \left. + C_{F21}^{(k,k'')} \tau_{21F} \left(C''_{22} \langle \beta_1' \beta_2^* \rangle + C''_{21} |\beta_1'|^2 \right) \right] |v_z|^2 \right\} \Big|_{k_y=0}. \end{aligned} \quad (48)$$

We use $\beta_2 = \sqrt{\kappa} \exp(i\theta) \beta_1$ to write $|\beta_2'|^2$, $\langle \beta_1^* \beta_2' \rangle$, and $\langle \beta_1' \beta_2^* \rangle$ in terms of $|\beta_1'|^2$. Assuming a steady state ($\partial/\partial t \rightarrow 0$), the zonal energy cancels from the balance, leaving

$$\nu = 2 \sum_{k'} \text{Re} \left[C_{F12}^{(k,k'')} \tau_{12F} \left(C''_{11} e^{i\theta} + C''_{12} \kappa \right) + C_{F21}^{(k,k'')} \tau_{21F} \left(C''_{22} e^{-i\theta} + C''_{21} \right) \right] |\beta_1'|^2 \Big|_{k_y=0}. \quad (49)$$

Equation (49) is a rigorous version of the approximate saturation-level expression given by Eq. (31) of Ref. [12]. Both expressions have the same scalings with ν , C_{F12} , τ_{ijF} , C_{iFj} and C_{ijF} , but Eq. (49) also accounts for $|\beta'_2|^2$, $\langle\beta'_1\beta'_2\rangle$, and $\langle\beta'_1\beta'^*_2\rangle$, whose values are known up to $\mathcal{O}(\hat{\epsilon}^8)$ in the expansion for small k and ν .

In Eq. (49), $|\beta'_1|^2$ is part of a sum. Numerical solutions show that the coupling coefficients and τ factors vary slowly relative to $|\beta'_1|^2$, which because of energy removal by stable modes drops sharply over the unstable wavenumber range. The coupling coefficients and τ factors can then be extracted from the sum (a Markovian approximation) leaving a sum over $|\beta'_1|^2$, which produces a spectrum-averaged value over the unstable wavenumber range. With $|\beta'_1|^2$ understood to be this average, Eq. (49) can be expressed as

$$|\beta'_1|^2 \sim \frac{\nu}{\sum_{k_x} \text{Re} \left\{ C_{F12}^{(k,k'')} [\tau_{21F} (C''_{21} + \sqrt{\kappa} C''_{22} e^{-i\theta}) + \tau_{12F} (\kappa C''_{12} + \sqrt{\kappa} C''_{11} e^{i\theta})] \right\}}, \quad (50)$$

where a sum over k_x is introduced to incorporate contributions from different zonal-flow wavenumbers. Note that in Ref. [10], the summation in Eq. (49) was approximated less consistently with spectrum features. However, because of the strong localization of fluctuation energy to the unstable wavenumber range, overall results are insensitive to these differences.

Equation (50) represents key aspects of ITG turbulence saturation. The factor ν in the numerator is the damping rate of the zonal flow. Larger zonal-flow damping requires stronger nonlinear energy transfer to the zonal flow to maintain the quasi-stationary state, leading to a higher turbulence level. The combination of the coupling coefficients and triplet correlation time in the denominator originates from the nonlinear energy transfer, which is proportional to the turbulence level. Larger values of the coupling coefficients and triplet correlation time produce more efficient nonlinear energy transfer and therefore lead to lower turbulence levels.

With $|\beta_1|^2$ given by Eq. (50), the heat flux as per Eq. (39) becomes

$$Q_i = \sum_{k'''} \frac{\gamma(k''')(1 + k''^2_{\perp})\nu(1 - \kappa)}{4\epsilon \sum_{k_x} (k'^2_{\perp} - k''^2_{\perp}) \text{Re} \left\{ ik'_y [\tau_{21F} (C''_{21} + C''_{22} \sqrt{\kappa} e^{-i\theta}) + \tau_{12F} (C''_{12} \kappa + C''_{11} \sqrt{\kappa} e^{i\theta})] \right\}}, \quad (51)$$

where $C_{F12}^{(k,k'')}$ is written explicitly using Eq. (21), thereby exposing a factor $(k'^2_{\perp} - k''^2_{\perp})$ in the denominator of Eq. (51). The combination of factors $\gamma(k''')/(k'^2_{\perp} - k''^2_{\perp})$ scales like the quasilinear

heat flux. The remaining factors constitute a nonlinear correction to quasilinear scaling. Critical nonlinear corrections include the triplet correlation times τ_{21F} and τ_{12F} , the coupling coefficients C''_{ij} , and the parameters κ and θ from the contributions of $|\beta_2|^2$ and $\langle\beta_1^*\beta_2\rangle$. The factor $1 - \kappa$ accounts for the up-gradient flux of the stable mode, in opposition to the down-gradient flux of the unstable mode. From Eq. (51), the heat flux is proportional to the zonal flow damping rate to a power -2 (since $\tau_{ijF} \propto \nu^{-1}$). The fact that the shearing paradigm of zonal-flow regulation [27] is also understood to produce a heat flux proportional to a positive power of ν [40] is coincidental. The latter requires a shearing rate that exceeds the nonlinear decorrelation rate by a sizable factor (~ 10 when zonal flow fluctuate), enhancing energy transfer to small scale turbulent fluctuations by boosting the turbulent decorrelation rate to the shearing level [2]. In zonal flow catalyzed transfer, straining by the zonal flow (the threshold-less shearing process of ordinary mode coupling) enhances transfer to large scale turbulent fluctuations by reducing the decorrelation rate to its smallest possible value.

Fig. 6 shows the heat flux and growth rate as functions of the temperature-gradient parameter η . The heat flux is calculated from a numerical solution of Eqs. (8) and (9) in conjunction with the analytic formula of Eq. (51) for a case with parameters $\epsilon = 1.25$, $\nu = 0.001$, and $\chi = 0$. Simulations were performed on a grid of 2048×1024 points in (k_x, k_y) , with $k_{x,\min} = 0.0125$ and $k_{y,\min} = 0.025$ in order to capture turbulent behavior for large η . A fourth order Runge-Kutta scheme was utilized. As for the heat flux evaluation from the analytic formula Eq. (51), k_x and k_y''' are summed over values from -0.25 to -0.15 and 0.25 to 0.4 , respectively. The triplet correlation times τ_{21F} and τ_{12F} are evaluated with the linear frequencies only, i.e., the eddy-damping decrements $\Delta\omega_j$ were neglected. According to Eq. (37), $\kappa \sim 1 - \nu k_\perp^2 / \gamma_2$ for k_\perp and ν small, making $1 - \kappa$ of order 10^{-4} in the low- k regime for η away from the linear threshold η_{crit} . In Fig. 6, the value $\kappa = 1 - 10^{-4}$ for higher η was assumed to represent η near threshold.

For comparison purposes, the scales of analytic and simulated heat fluxes in Fig. 6 are adjusted so that the two curves coincide at the highest value of η . We observe that both fluxes have positive curvature, in contrast to the negative curvature of the growth rate, giving a region above the

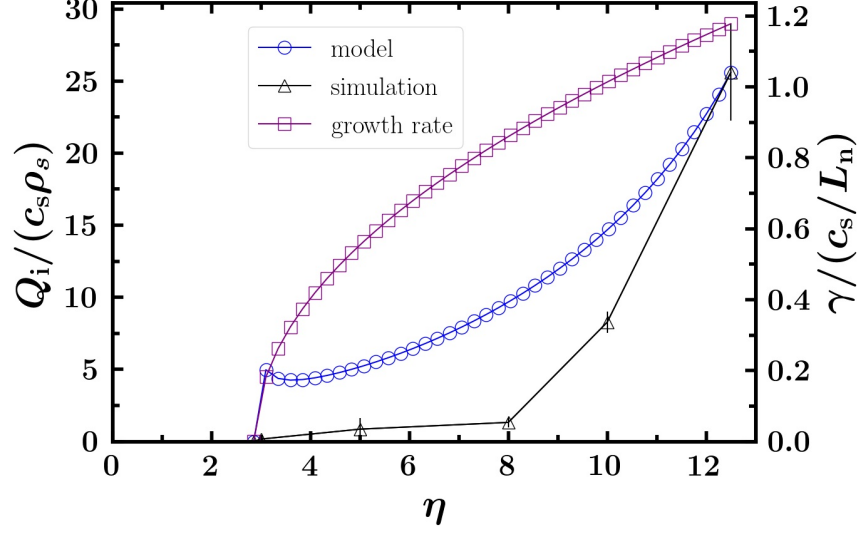


Figure 6: Growth rate at $\mathbf{k} = (0, 0.25)$ (magenta), analytic heat flux (blue) and simulated heat flux (black) as a functions of η for $\epsilon = 1.25$, $\nu = 0.001$ and $\chi = 0$. Eddy damping is neglected in the triplet correlation time factors of the analytic formula. The heat flux predicted from the analytic formula showing unphysical behavior close to the linear threshold.

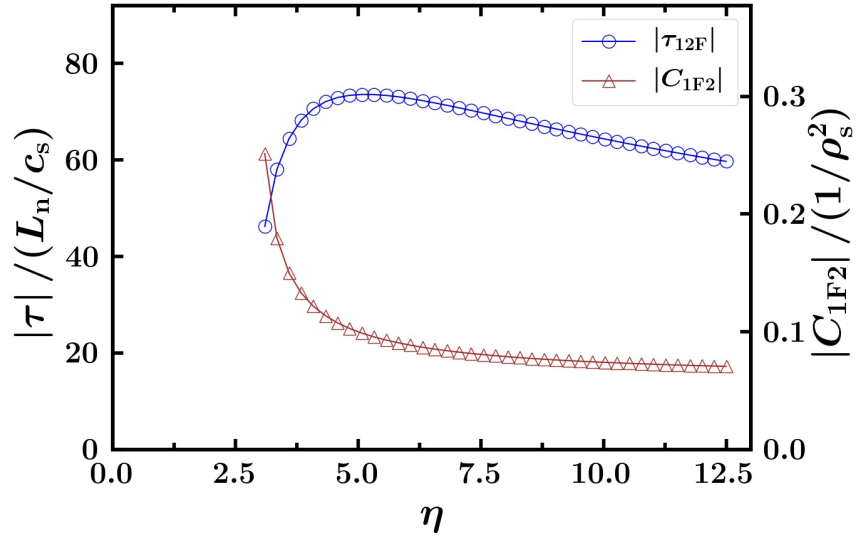


Figure 7: Triplet correlation time (blue) and coupling coefficient C_{1F2} (red) as a function of η for the same parameters as Fig. 6. Eddy damping is neglected in $|\tau|$. The triplet correlation time increases dramatically just above the linear threshold, which leads to the spike of the heat flux in close-threshold region.

threshold where heat flux increases slowly before turning up more sharply. The analytic flux has an unphysical spike just above the threshold which artificially raises its value relative to the simulated flux. This spike arises from a prompt increase of τ above the threshold followed by a slow slide off at higher η , as shown in the blue trace of Fig. 7. This behavior is unphysical because increasing η , which increases the dispersive components of frequencies and growth rates, necessarily *decreases* τ immediately above threshold. The source of the unphysical increase of τ is traced to the fact that the k dependence of the threshold puts multiple thresholds into τ from its frequencies at different wavenumber. This creates the spike region near the threshold in which the crossing of the identities of stable and unstable produce an increase in τ .

This sensitivity to a two-mode representation of the eigenmode space can be expected to be smoothed by eddy damping. This nonlinear frequency-broadening process is important near threshold, where resonance makes $\omega''_2 + \omega'_1 - \omega_1^*$ much smaller than individual frequencies, bringing eddy damping into prominence even in the low-amplitude threshold regime. Moreover, Eq. (46) shows that the dominant component of the eddy damping $\Delta\omega$ is proportional to the product of $|v_z|^2$ and $C_{jF}C_{j|F}$. The coefficient C_{1F2} is plotted in Fig. 7 as the red line, where it is seen that C_{1F2} is largest near the threshold. This behavior arises from the form $C_{1F2} \propto [\text{Re}(\omega) + i\gamma]/\gamma$, which makes C_{1F2} strongest just above the threshold where $\text{Re}(\omega) \gg \gamma$ and $C_{iFj} \propto \text{Re}(\omega)/\gamma \gg 1$. At large η , the coupling coefficient C_{1F2} asymptotes to a smaller constant. The importance of eddy damping near resonance is amplified near threshold by this effect and therefore should not be ignored.

Fig. 8 shows that by adding the eddy damping rate $\Delta\omega$ of Eq. (46) to the τ factors of Eq. (51), the countering trends of τ in Fig. 6 are removed, thereby smoothing the unphysical behavior of Q_i around the instability threshold. The predicted heat flux now agrees much better with the simulation starting from the linear threshold. In Fig. 9, the triplet correlation time with eddy damping included is plotted as a function of η , showing that the triplet correlation time decreases monotonically with η , as expected for nearly resonant frequencies that increase with η . This behavior represents a resonance in the standard sense of turbulent mode-coupling interactions. We note that the decrease of coupling coefficient with η , shown in Fig. 9 for comparison, is also

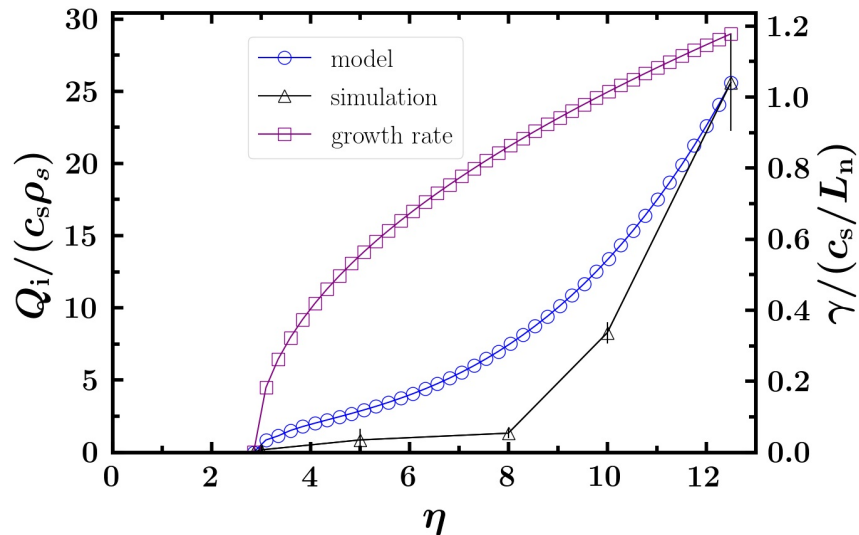


Figure 8: Growth rate (magenta), analytic heat flux (blue), and simulated heat flux (black) as functions of η for $\epsilon = 1.25$, $\nu = 0.001$, and $\chi = 0$, with eddy damping included in the analytic formula.

pronounced, significantly contributing to the suppression of the heat flux immediately above the threshold. This effect can also be termed as resonant because it arises from the dependence of C_{1F2} on mode frequency, describing an enhancement of zonal-flow-mediated coupling between stable and unstable modes just above threshold.

The behavior depicted in Fig. 9 is broadly consistent with critical features of the Dimits shift. No bifurcation is observed, but rather a continuously increasing slope from a region near the instability threshold with very low flux. The match of the analytic flux with the simulated flux is not perfect, but the former generally tracks the variation of the latter. Both differ decidedly from the variation of the growth rate with η . The features evident in Fig. 9 are replicated for other parameter values. Figure 10 shows the heat flux versus η for $\epsilon = 1.25$ and $\epsilon = 0.625$. As the magnetic curvature parameter, the threshold depends on ϵ . In Fig. 10, the simulated heat flux is actually larger than the analytic flux near the threshold for $\epsilon = 0.625$, and it is clearly evident that while there is noticeable upturn in slope of simulated heat flux at $\eta = 8$, the flux below that value is not zero. Variations with collisionality, which produce consistent effects in gyrokinetics and the present fluid model, will be described in a separate gyrokinetic study, along with other

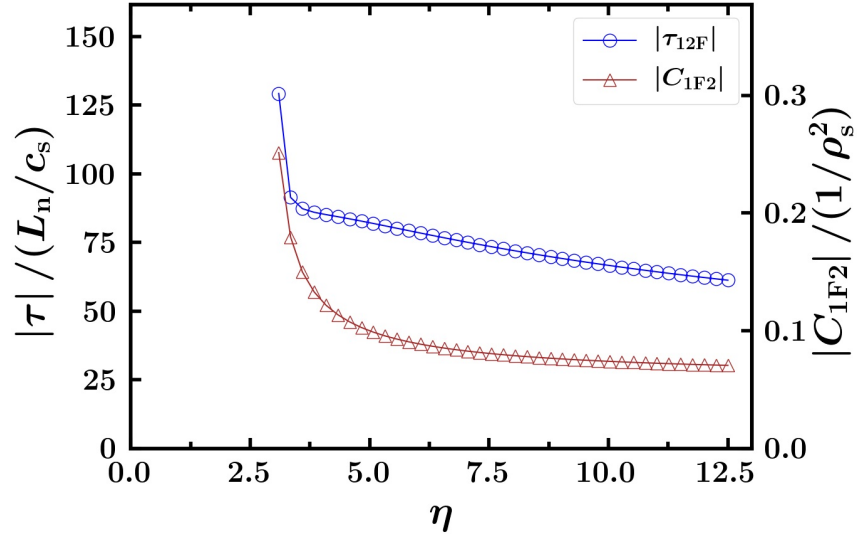


Figure 9: Triplet correlation time (blue) and coupling coefficient C_{1F2} (red) as a function of η for the same parameters as Fig. 4 with eddy damping included in τ . The triplet correlation time decreases monotonically as η increases, which eliminates the unphysical behavior.

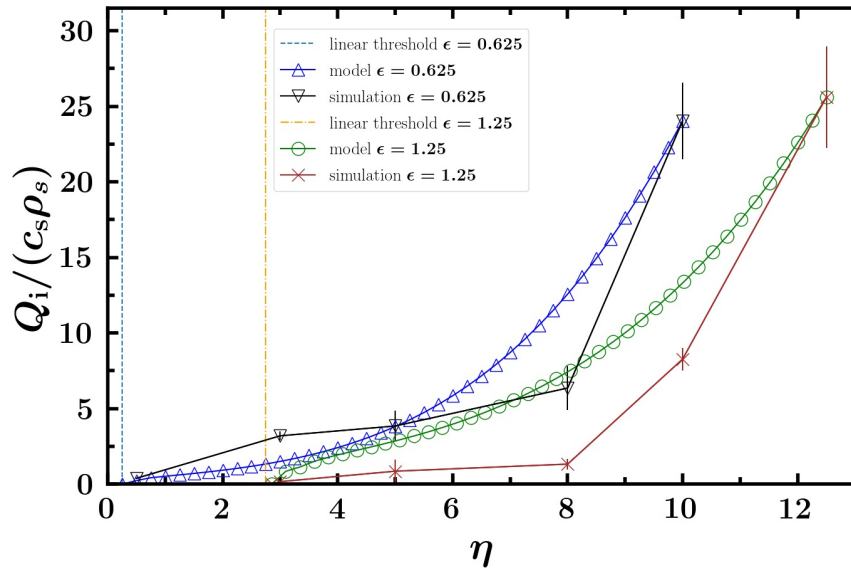


Figure 10: Heat flux as a function of η for $\epsilon = 0.625$ and $\epsilon = 1.25$ analytic theory (triangles and circles), numerical solution (inverted triangles and crosses).

tests that directly broaden the resonance in the triplet correlation time. These modifications result in a increase in the heat flux and generally support the conclusion that resonance is an important aspect of the critical gradient upshift. The idea of resonant interactions has been used to modify quasilinear modeling, which in standard formulations does not capture the resonant aspects of saturation. The result is an improved quasilinear model that is able to capture the critical gradient upshift in gyrokinetic simulations [39].

7 Conclusions

Physics central to the Dimits shift, a phenomenon where the ion heat flux becomes significant only at a larger temperature gradient than the critical gradient of linear instability, has been analyzed with approaches based on gyrokinetic simulation and fluid-model analytic theory. The simulations show that fluctuations and transport are not zero between the linear instability threshold and the nonlinear critical gradient (NLCG) where the flux rises sharply. Accordingly, turbulent transfer was investigated in the regimes of low and high transport on either side of the NLCG. Instantaneous nonlinear spectral energy transfer and scale-to-scale-cascaded energy transfer were found to be similar in both regimes, differing essentially in magnitude only. Energy transfer is governed by zonal-flow-catalyzed mode coupling — the interaction between the unstable mode, a stable mode, and the zonal flow at a triplet of wavenumbers.

A saturation theory based on this interaction was extended from the strong-transport regime for which it was originally developed to the weak-transport regime near the linear threshold by building the kinetic threshold of the ITG instability into the fluid model. The dominant mode coupling is resonant for $k_{\perp}^2, \nu \rightarrow 0$, i.e., the frequency mismatch of the triplet correlation time is zero because the stable mode forms a conjugate pair with the unstable mode and the zonal flow is a zero-frequency mode. This allows maximally efficient transfer to the stable-mode energy sink, yielding negligibly low levels of fluctuations and transport for a given instability growth rate. The resonance is broadened by finite ν , k_{\perp}^2 , and eddy damping, producing a small heat flux near the instability threshold. The minimum value of the triplet correlation time produced by the broadening

grows with temperature gradient, allowing the flux to become significant after a gradient range of latency set by the broadening.

Adequate description of this physics requires accounting for nonlinear transfer between eigenmodes, with the heat flux depending on the eigenmode auto and cross correlations $|\beta_1|^2$, $|\beta_2|^2$ and $\langle\beta_1^*\beta_2\rangle$. Expressions were derived for the relationship between these correlations. Because of the near conjugate symmetry in the regime k_\perp^2 , $\nu \ll 1$, these relationships are dominated by linear physics in steady state. The contribution of $|\beta_2|^2$ to transport is significant and nearly cancels the quasilinear contribution from $|\beta_1|^2$, while $\langle\beta_1^*\beta_2\rangle$ makes a negligible contribution. The level of $|\beta_2|^2$ is set by equipartition of energy injection and removal rates $\gamma_1|\beta_1|^2$ and $\gamma_2|\beta_2|^2$.

The nonlinear balance for zonal-flow energy determines $|\beta_1|^2$ since the zonal energy drops out for zonal-flow-catalyzed mode coupling. This balance was solved inclusive of all eigenmode correlations by Markovianizing its nonlinear convolution and summing over wavenumber. The flux and $|\beta_1|^2$ are proportional to ν , the inverse of the triplet correlation time, and the inverse of a product of coupling coefficients. The eigenmode-frequency dependence of one of these coefficients gives it resonant behavior, i.e., it decreases sharply above the linear instability threshold. The heat-flux dependence on the nearly resonant triplet correlation time also explains to a substantial degree the nonlinear finite- β stabilization of ITG turbulence.

This theory does not account for all processes that may have bearing on the critical-gradient upshift. Turbulent fluctuations are intermittent just above the linear-instability threshold due to the relative paucity of mode coupling interactions available under the vanishing growth rate and instability range. Intermittency challenges the assumptions of closure calculations, although the one used here explicitly accounts for the weak-turbulence limit by retaining the resonance of three-wave interactions. This theory accounts only for the zonal-flow-catalyzed interaction. Well above the linear critical gradient, other nonzonal mode mode-coupling interactions may eventually become prominent. This theory does not apply when such interactions are dominant. Strongly ballooning modes in the ballooning representation of toroidal geometry are also assumed, limiting consideration of nonlinear eigenmode structure evolution not amenable to spectral representation.

Non-adiabatic electrons have been omitted in keeping with the simplest realization of ITG physics. Non-adiabatic electrons are related to trapped electron mode (TEM) physics, where a critical gradient upshift has been noted in the density-gradient driven case [41]. Improvements of earlier work [42] on stable modes and zonal flows in TEM turbulence are under development and will be reported elsewhere. Mean flow shear has also been neglected. Its inclusion could be of interest for studying the interaction of the distinct processes of shear suppression by an externally maintained shear flow and saturation by zonal-flow-catalyzed transfer.

Acknowledgments

This work was supported by U.S. Department of Energy Grant DE-FG02-89ER53291. The data supporting the findings of this study is available from the authors upon reasonable request.

References

- [1] W. Horton, Rev. Mod. Phys. **71**, 735 (1999).
- [2] P.W. Terry, Rev. Mod. Phys. **72**, 109 (2000).
- [3] E. J. Strait, L. L. Lao, M. E. Mauel, B. W. Rice, T. S. Taylor, K. H. Burrell, M. S. Chu, E. A. Lazarus, T. H. Osborne, S. J. Thompson et al., Phys. Rev. Lett. **75**, 4421 (1995).
- [4] D.E. Newman, B.A. Carreras, D. Lopez-Bruna, P.H. Diamond, and V.B. Lebedev, Phys. Plasmas **5**, 938 (1998).
- [5] J.W. Hughes, N.T. Howard, P. Rodriguez-Fernandez, A.J. Creely, A.Q. Kuang, P.B. Snyder, T.M. Wilks, R. Sweeney, and M. Greenwald, J. Plasma Phys. **86**, 865860504 (2020).
- [6] H.E. Mynick, N. Pomphrey, and P. Xanthopoulos, Phys. Rev. Lett. **105**, 095004).
- [7] C.C. Hegna, P.W. Terry and B.J. Faber, Phys. Plasmas **25**, 022511 (2018).
- [8] A.M. Dimits, G. Bateman, M.A. Beer, B.I. Cohen, W. Dorland, G.W. Hammett, C. Kim, J.E. Kinsey, M. Kotschenreuther, A.H. Kritz et al., Phys. Plasmas, **7**, 969 (2000).

- [9] D.R. Mikkelsen and W. Dorland, Phys. Rev. Lett. **101**, 135003 (2008).
- [10] P.W. Terry, P.-Y. Li, M.J. Pueschel, and G.G. Whelan, Phys. Rev. Lett. **126**, 025004 (2021).
- [11] Z.R. Williams, M.J. Pueschel, P.W. Terry, and T. Hauff, Phys. Plasmas **24**, 122309 (2017).
- [12] P.W. Terry, B.J. Faber, C.C. Hegna, V.V. Mirnov, M.J. Pueschel, and G.G. Whelan, Phys. Plasmas **25**, 012308 (2018).
- [13] B.N. Rogers, W. Dorland, and M. Kotschenreuther, Phys. Rev. Lett. **85**, 5336 (2000).
- [14] K. Miki, Y. Kishimoto, N. Miyato, and J.Q. Li, Phys. Rev. Lett. **99**, 145003 (2007).
- [15] S.-I. Itoh and K. Itoh, Nucl. Fusion **56**, 106028 (2016).
- [16] F. Rath, A.G. Peeters, R. Buchholz, S.R. Grosshauser, F. Seiferling, and A. Weikl, Phys. Plasmas **25**, 052102 (2018).
- [17] C. Holland, P.H. Diamond, S. Champeaux, E. Kim, O. Gurcan, M.N. Rosenbluth, G.R. Tynan, N. Crocker, W. Nevins, and J. Candy, Nucl. Fusion **43**, 761 (2003).
- [18] D.A. St-Onge, J. Plasma Phys. **83**, 905830504 (2017).
- [19] H. Zhu, Y. Zhou, and I.Y. Dodin, Phys. Rev. Lett. **124**, 055002 (2020).
- [20] K. Makwana, P.W. Terry, and J.-H. Kim, Phys. Plasmas **19**, 062310 (2012).
- [21] K. Makwana, P.W. Terry, M.J. Pueschel, and D.R. Hatch, Phys. Rev. Lett. **112**, 095002 (2014).
- [22] M. Stransky, Phys. Plasmas **18**, 052302 (2011).
- [23] D.R. Hatch, P.W. Terry, F. Jenko, F. Merz, and W.M. Nevins, Phys. Rev. Lett. **106**, 115003 (2011).
- [24] P.W. Terry, K.D. Makwana, M.J. Pueschel, D.R. Hatch, F. Jenko, and F. Merz, Phys. Plasmas **21**, 122303 (2014).

- [25] D.R. Hatch, P.W. Terry, F. Jenko, F. Merz, M.J. Pueschel, W.M. Nevins, and E. Wang, *Phys. Plasmas* **18**, 055706 (2011).
- [26] G.G. Whelan, M.J. Pueschel, and P.W. Terry, *Phys. Rev. Lett.* **120**, 175002 (2018).
- [27] P.H. Diamond, S.-I. Itoh, K. Itoh, and T.S. Hahm, *Plasma Phys. Control. Fusion* **47**, R35 (2005).
- [28] F. Jenko, W. Dorland, M. Kotschenreuther, and B.N. Rogers, *Phys. Plasmas* **7**, 1904 (2000).
- [29] G. Hammett, UCLA Winter School, Center for Multiscale Plasma Dynamics, Los Angeles, CA, Jan. 2007.
- [30] G.G. Whelan, Ph.D. Dissertation, Univ. of Wisconsin-Madison, 2019.
- [31] W. Horton, D.-I. Choi, and W.M. Tang, *Phys. Fluids* **24**, 1077 (1981).
- [32] M.J. Pueschel and F. Jenko, *Phys. Plasmas* **17**, 062307 (2010).
- [33] G.G. Whelan, M.J. Pueschel, P.W. Terry, J. Citrin, I.J. McKinney, W. Guttenfelder, and H. Doerk, *Phys. Plasmas* **26**, 082302 (2019).
- [34] A.J. Wootton, M.E. Austin, R.D. Bengtson, J.A. Boedo, R.V. Bravenec, D.L. Brower, J.Y. Chen, G.Cima, P.H. Diamond, R.D. Durst et al., *Plasma Phys. Control. Fusion* **30**, 1479 (1988).
- [35] S.A. Orszag, *J. Fluid Mech.* **41**, 363 (1970).
- [36] R.H. Kraichnan, *J. Fluid Mech.* **5**, 497 (1959).
- [37] P.W. Terry and W. Horton, *Phys. Fluids* **26**, 206 (1983).
- [38] M.J. Pueschel, M. Kammerer and F. Jenko, *Phys. Plasmas* **15**, 102310 (2008).
- [39] M.J. Pueschel, P.-Y. Li and P.W. Terry, *Nucl. Fusion* **61**, 054003 (2021).

- [40] Z. Lin, T.S. Hahm, W.W. Lee, W.M. Tang, and P.H. Diamond, Phys. Rev. Lett. **83**, 3645 (1999).
- [41] D.R. Ernst, J. Lang, W.M. Nevins, M. Hoffman, Y. Chen, W. Dorland, and S. Parker, Phys. Plasmas **16**, 055906 (2009).
- [42] R. Gatto, P.W. Terry, and D.A. Baver, Phys. Plasma **13**, 022306 (2006).